Large random arrowhead matrices: Multifractality, semilocalization, and protected transport in disordered quantum spins coupled to a cavity

J. Dubail,[1,2,*] T. Botzung,[2,3,4] J. Schachenmayer,[2] G. Pupillo,[2,5,†] and D. Hagenmüller[2,‡]

[1]*LPCT (UMR 7019), Université de Lorraine and CNRS, 54000 Nancy, France*
[2]*ISIS (UMR 7006), and icFRC, Université de Strasbourg and CNRS, 67000 Strasbourg, France*
[3]*Institute for Quantum Information, RWTH Aachen University, 52056 Aachen, Germany*
[4]*Institute for Theoretical Nanoelectronics (PGI-2), Forschungszentrum Jülich, 52428 Jülich, Germany*
[5]*Institut Universitaire de France, 75000 Paris, France*

(Received 25 May 2021; revised 14 January 2022; accepted 24 January 2022; published 22 February 2022)

Large arrowhead matrices with randomly distributed entries describe a variety of important phenomena where a degree of freedom is nonlocally coupled to a disordered continuum of modes, including central-spin problems in condensed matter, molecular junctions, and quantum emitters in cavity QED. Here we provide an exact solution of random arrowhead Hamiltonians with diagonal disorder in the thermodynamic limit. For concreteness, we focus on the problem of N emitters homogeneously coupled to a nonlocal cavity mode, corresponding to the disordered Tavis-Cummings model of cavity QED in the single-excitation limit, for which we provide asymptotically exact formulas for static and dynamical quantities of interest. By varying the coupling strength, we find that the distribution of energy spacing can be continuously tuned between Poisson statistics and a distribution that is very close to semi-Poisson statistics, the latter statistics being usually associated with the critical point of Anderson localization-delocalization transitions. We show that the system has a peculiar diffusivelike behavior with an escape probability growing linearly with time for any finite coupling strength and that the escape rate can be controlled by selecting the energy of the initial site. The escape rate averaged over the disorder configurations is found to exhibit a maximum for intermediate coupling strengths, before saturating at a lower, g-independent value for sufficiently large N in the collective strong-coupling limit, a cavity protection effect. We investigate the system in a two-terminal configuration and show that the steady-state excitation current exhibits features similar to the escape probability, thereby extending our cavity-protected transport scenario to out-of-equilibrium situations. We finally demonstrate that dark states can provide a major contribution to long-distance transport in disordered systems.

DOI: 10.1103/PhysRevA.105.023714

I. INTRODUCTION

Random Hamiltonians involving N degrees of freedom are typically described by $N \times N$ Hermitian matrices with matrix elements that are independent and identically distributed variables. As originally suggested by Wigner, looking at the statistical properties of the distribution of eigenvalues in the large-N limit can be relevant in physics [1–5]. Random arrowhead [6–9] or bordered diagonal [10,11] matrices are particularly simple examples of random matrices having most of their matrix elements equal to zero except the ones along the diagonal and along the last line and last column.

Large random arrowhead matrices naturally appear in the common physical situation where a specific degree of freedom is nonlocally coupled to a randomly disordered continuum of modes acting as an environment (see Fig. 1) [12]. Among the broad variety of possible physical systems, this occurs, for instance, in molecular junctions, where a localized vibrating molecule interacts with the free-electron gas of a metallic surface placed in close proximity [13,14] [see Fig. 2(a)]. The random arrowhead Hamiltonian model is here highly relevant to describe charge [16–18] and heat [19–21] currents flowing through the junction. Other related situations are plasmonic nanogap junctions [22], semiconductor quantum point contacts [23,24], and a single molecule embedded in a plasmonic nanocavity [22,25]. This model is also useful in central-spin problems, where a single (central) spin nonlocally interacts with a spin bath of localized modes [26–28]. Recent developments of quantum computation with solid-state qubits such as quantum dots [29,30] [see Fig. 2(b)], superconducting qubits [31], and nitrogen-vacancy centers in diamond [32] have revived interest in this model, where proper understanding of the decoherence mechanisms affecting the central spin is of crucial importance.

Other important examples of random arrowhead Hamiltonians arise in cavity QED. In this case the central site approximates a bosonic mode of the electromagnetic field, which can be confined in either an optical cavity [33,34] or a plasmonic structure [35] and is nonlocally coupled to N quantum emitters (two-level systems) described by local pseudospin operators with coupling strength g [see Fig. 2(c)].

*jerome.dubail@univ-lorraine.fr
†pupillo@unistra.fr
‡dhagenmuller@unistra.fr

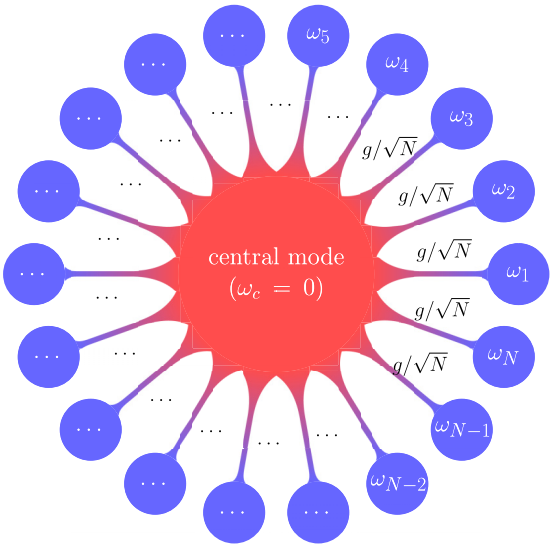

FIG. 1. Random arrowhead Hamiltonians appear when a specific (central) degree of freedom with energy ω_c is nonlocally coupled to a randomly disordered ensemble of N modes with energies $\omega_1, \omega_2, \ldots, \omega_N \in [-W/2, W/2]$ (W is the disorder strength), those energies forming a continuum in the thermodynamic limit $N \to \infty$. Without loss of generality, the energy of the central mode can be set to zero. In this paper, we focus on the situation with uniform couplings $g/\sqrt{N}$ between the central mode and all the others.

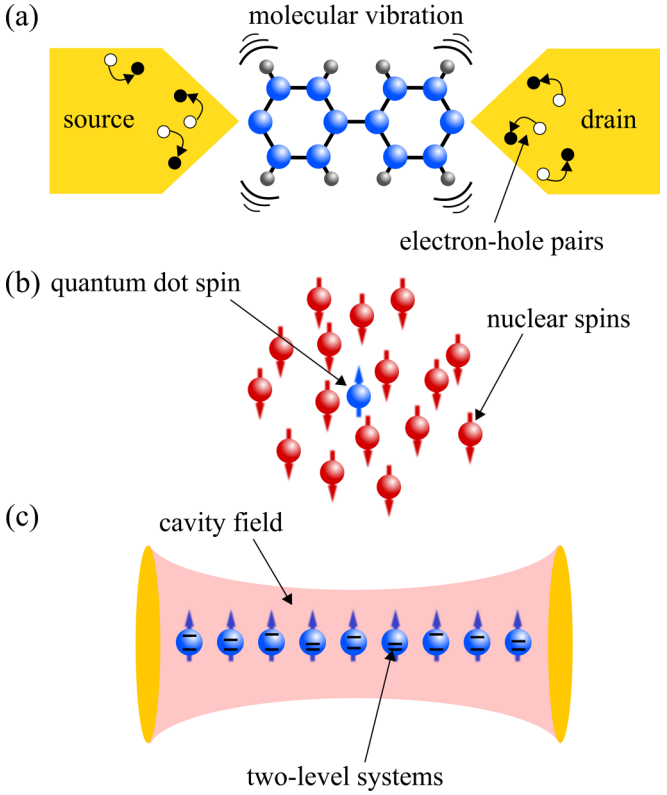

FIG. 2. Physical realizations of random arrowhead Hamiltonians. (a) Molecular junction consisting of a single molecule coupled to metallic leads for charge and thermal transport (adapted from Ref. [15]). The central (bosonic) mode corresponds to molecular vibrations, which interact with two disordered continua of electron-hole pairs in the leads. (b) A central quantum dot with a single electron of spin $+\frac{1}{2}$ is inhomogeneously coupled to an ensemble of polarized nuclear spins $-\frac{1}{2}$ via hyperfine interaction. (c) Cavity QED setup consisting of a central cavity electromagnetic (bosonic) mode coupled to an inhomogeneously broadened ensemble of two-level systems (pseudospins), which is the focus of this paper.

In the common situation where the transition frequencies of these two-level systems are inhomogeneously broadened (calling W the bandwidth), one ends up with a disordered version of the famous Tavis-Cummings (TC) model [36]. The TC model has been realized in a variety of physical systems, including superconducting qubits [37,38], nitrogen-vacancy centers in diamond [39,40], and atomic systems [34,41–44], with recent implementations focusing on Raman laser dressing of four-level atoms trapped in a cavity optical lattice [43–45].

The disordered TC model and other closely related models for quantum-well exciton polaritons have already been looked at to study the effect of inhomogeneous broadening on the polariton spectrum [46–50] and on superradiance [51]. Similar models including a hopping term between nearest-neighbor sites were also studied [52,53] in connection to recent experiments on transport through molecular materials strongly coupled to light [54–56]. In this case, diagonal disorder (inhomogeneous broadening of molecular excitons), off-diagonal disorder (inhomogeneous hopping) [57], and orientational disorder [58] leading to inhomogeneous couplings to the cavity electric field are all expected to play an important role and cannot *a priori* be neglected. Theoretical investigations on the nontrivial interplay between disorder and strong light-matter coupling are therefore highly desirable for further developments of polaritonic material science.

In Ref. [59] we studied numerically the disordered TC model in the presence of additional hopping of spin excitations between nearest-neighboring sites. The purpose of including such a hopping term was to investigate the effect of the spin-cavity coupling on the metal-insulator Anderson transition [60,61]. It was shown that the cavity mode strongly modifies the localization properties of the eigenstates, which feature the novel character of being localized on multiple noncontiguous sites, a behavior we dubbed semilocalization. It was also shown that those semilocalized eigenstates can efficiently contribute to coherent energy transport under strong-coupling conditions, i.e., when the collective coupling strength g exceeds the bandwidth of the disordered spin ensemble. Such cavity-induced robustness of transport and delocalization against disorder was also highlighted in other very recent works [62–64], showing a growing interest in cavity-protected transport.

Here we present a detailed analysis of the disordered TC model (without hopping) in the single-excitation subspace, providing asymptotically exact formulas for the spectrum, average energy shifts induced by the coupling to the cavity mode, and correlation functions for all coupling strengths g/W. In particular, we show that the distribution of energy spacings can be continuously tuned between Poisson statistics and a distribution very close to semi-Poisson statistics for

$g/W \gg 1$, the latter statistics usually being associated with the critical point of Anderson localization-delocalization transitions. We also demonstrate that all the eigenstates consisting of polaritons and a continuum of dark states are multifractal. This indicates the existence of a critical semilocalized phase for all values of g/W, where the dark states are localized over multiple noncontiguous sites. The dark-state multifractal spectrum and anomalous dimension are found to be identical to those of the critical point of the Anderson model on the Bethe lattice, which is commonly regarded as a mean-field model (dimension $d \to \infty$) of the localization-delocalization transition.

Later in the paper we explain how the spectral properties of the model can be harnessed to engineer transport through the system of emitters. We show that the escape probability of an excitation from some given site grows linearly with time for any finite coupling strength g, similarly to a diffusive motion, and that the escape rate can be fully controlled by tuning the energy of the initial excitation across the disorder distribution. We provide a Fermi-golden-rule-based interpretation of these results using second-order perturbation theory, where the nonlocal coupling of the emitters to the cavity mode leads to an effective long-range hopping with amplitude depending only on the disordered energies of the emitters, but not on the distance between them. We show that the disorder-averaged escape rate exhibits a maximum for intermediate values of the coupling strength $g/W \sim 1$, before saturating to a lower, g-independent value for strong couplings $g/W \gg 1$, a cavity-protection effect of transport that could find important applications in, e.g., optoelectronic devices. Surprisingly, we find that the saturation value increases with the disorder strength, which indicates that not only does the cavity protect transport against disorder, but the latter can also contribute favorably to transport provided the light-matter coupling is strong enough. We also compute the steady-state excitation current when coupling the system to two external leads, with relevance to mesoscopic physics experiments. In contrast to common expectations from polaritonics, we demonstrate that out-of-equilibrium transport is fully dominated by the contribution of the dark states. The role the latter has played in influencing dynamics has been attracting more and more interest as a possible key aspect of polaritonic material science and polaritonic chemistry [59,62,63,65,66].

The disordered TC model under consideration is described by the Hamiltonian $\hat{H} = \hat{H}_0 + \hat{V}$, with

$$\hat{H}_0 = \sum_{i=1}^{N} \omega_i \hat{\sigma}_i^+ \hat{\sigma}_i^- + \omega_c \hat{a}^\dagger \hat{a},$$

$$\hat{V} = \frac{g}{\sqrt{N}} \sum_{i=1}^{N} (\hat{a}\hat{\sigma}_i^+ + \hat{\sigma}_i^- \hat{a}^\dagger). \tag{1}$$

The first term $\hat{H}_0$ provides the energy of the disordered spin ensemble and the cavity mode, with $\hat{\sigma}_i^-$ ($\hat{a}$) and $\hat{\sigma}_i^+$ ($\hat{a}^\dagger$) the ith spin (cavity) annihilation and creation operators, respectively. The cavity-mode energy ω_c can here be set to zero without loss of generality. The second term describes the coupling between the spins and the cavity. Note that while the uniform coupling assumption would not be *a priori* suitable for a molecular ensemble, it is well justified in a scheme using ultracold atoms, where the laser beam waist creating the lattice potential is typically much broader than the atomic ensemble [43,44]. In this paper we consider the coupling uniform and leave the interesting situation with inhomogeneous coupling for future investigations. Since the scaling of the coupling with N comes from its dependence on the cavity-mode volume V as $\sim 1/\sqrt{V}$ [67], the collective coupling strength g is the relevant physical parameter in the thermodynamic limit $N \to \infty$ as it remains independent of N for a fixed density N/V.

The Hamiltonian (1) commutes with the excitation number operator $\hat{N} = \sum_i \hat{\sigma}_i^+ \hat{\sigma}_i^- + \hat{a}^\dagger \hat{a}$. In the single-excitation subspace, the number operator is thus represented as an identity matrix and this subspace is spanned by the $N+1$ eigenstates of H_0, $\{|i,0\rangle, |G,1\rangle\}$, where $|i,0\rangle$ has the ith spin in its excited state and $|G,1\rangle$ has all spins in their ground state and one photon in the cavity. In this basis, the Hamiltonian takes the arrowhead matrix form

$$H = \left(\begin{array}{ccccccc|c} \omega_1 & 0 & & & \dots & 0 & & g/\sqrt{N} \\ 0 & \omega_2 & 0 & & & & & \\ & 0 & \ddots & \ddots & & \vdots & & \\ \vdots & & \ddots & & 0 & & & \vdots \\ & & & 0 & \omega_{N-1} & 0 & & \\ 0 & & \dots & & 0 & \omega_N & & g/\sqrt{N} \\ \hline g/\sqrt{N} & & & \dots & & g/\sqrt{N} & & 0 \end{array}\right), \tag{2}$$

where the bare energies ω_j, $j = 1, \dots, N$, are independent and identically distributed random variables, drawn from a probability distribution $\rho(\omega)$ [with $\int \rho(\omega) d\omega = 1$] such that the density of bare energies

$$\sum_{j=1}^{N} \delta(\omega - \omega_j) \underset{N\to\infty}{\simeq} N\rho(\omega) \tag{3}$$

in the thermodynamic limit. For simplicity, we assume that $\rho(\omega)$ is supported on an interval $[\omega_{\min}, \omega_{\max}]$. We write $\mathbb{E}[\cdot]$ for the expectation value taken with respect to the probability distribution $\rho(\omega)$, i.e.,

$$\mathbb{E}[O(\{\omega_j\})] = \int \left(\prod_{i=1}^{N} \rho(\omega_i) d\omega_i\right) \mathcal{O}(\{\omega_j\}) \tag{4}$$

for any observable. $\mathcal{O}(\{\omega_j\})$, and we refer to it as the disorder average. Throughout the paper, we work with a general function $\rho(\omega)$ supported on the interval $[\omega_{\min}, \omega_{\max}]$. However, for comparison with numerics we find that it is convenient to specialize to the case of a box distribution, i.e., the uniform distribution with $\rho(\omega) = 1/W$ for $\omega \in [-W/2, W/2]$ and $\rho(\omega) = 0$ otherwise; W thus quantifies the disorder strength.

Important insights can be gained by writing the Hamiltonian (1) in terms of the collective Fourier operators $\hat{b}_q = \frac{1}{\sqrt{N}} \sum_j \hat{\sigma}_j^- e^{iqj}$, with $q = 0, 1, \dots, N-1$ [52]. These operators are bosonic in the single-excitation subspace since

$$\langle G, 0 | [\hat{b}_q, \hat{b}_{q'}^\dagger] | G, 0 \rangle = \delta_{q,q'}.$$

Let us assume for clarity that the bare energies ω_j are distributed around a mean value $\overline{\omega} = \frac{1}{N}\sum_i \omega_i \neq 0$, i.e., $\omega_j \in [\overline{\omega} - W/2, \overline{\omega} + W/2]$. In this case the Hamiltonian (1) takes the form

$$\hat{H} = \overline{\omega}\hat{b}_0^\dagger \hat{b}_0 + \omega_c \hat{a}^\dagger \hat{a} + g(\hat{a}\hat{b}_0^\dagger + \hat{b}_0 \hat{a}^\dagger) + \overline{\omega}\sum_{q\neq 0} \hat{b}_q^\dagger \hat{b}_q + \sum_{q\neq q'} U_{q,q'} \hat{b}_q^\dagger \hat{b}_{q'}, \tag{5}$$

with $U_{q,q'} = \frac{1}{N}\sum_j \omega_j e^{i(q-q')j}$. At resonance ($\overline{\omega} = \omega_c$), the first line of Eq. (5) can be diagonalized by the two polariton eigenmodes $\hat{p} = (\hat{b}_0 \pm \hat{a})/\sqrt{2}$ with energies $\overline{\omega} \pm g$, separated by the Rabi splitting $2g$ in analogy with the Autler-Townes effect for driven two-level systems [67]. The polaritons thus consist of a mix between cavity photons and the collective homogeneous spin mode $q = 0$ often called the bright mode. Note that the polariton energies are simply $\pm g$ when setting $\overline{\omega} = 0$ as in the rest of the paper.

In the absence of disorder, i.e., when all bare energies are equal to $\overline{\omega}$, the last term proportional to $U_{q,q'}$ in the second line of Eq. (5) vanishes and the spectrum thus consists of the two polaritons plus $N - 1$ dark modes with energy $\overline{\omega}$ that do not interact with the cavity mode. A finite bandwidth W for the disorder distribution changes this picture as the term proportional to $U_{q,q'}$ leads to a scattering between the different Fourier modes. In particular, the term $U_{0,q}$ is responsible for a coupling of the dark modes to cavity photons via the bright mode $q = 0$. Dark states are thus expected to acquire a finite photon weight due to the presence of disorder, as was already pointed out in Refs. [54,59,65]. Although polaritons and dark modes are not exact eigenmodes of the Hamiltonian in the presence of disorder, we will see in the following that the spectrum can however be understood similarly in those terms.

A. Summary of the results

Having introduced the model and its underlying physical motivations, we now provide a summary of the main results of this paper.

1. Spectrum and energy shifts

In Sec. III we analyze the spectrum of the Hamiltonian H and derive an asymptotically exact formula at large N for the average energy shift of the disordered energy levels of the emitters induced by the coupling to the cavity. We find that the spectrum consists of two modes with unbounded energies ε_+ and ε_- outside the interval $[\omega_{\min}, \omega_{\max}]$, the support of $\rho(\varepsilon)$. For weak couplings (e.g., $g \ll W$ for a box disorder distribution of width W) these modes are parametrically close to the edges of the distribution at $\omega_{\min}$ and $\omega_{\max}$ and contain a vanishing photon weight. In contrast, for strong couplings ($g \gg W$), they are hybrid modes composed of 50% cavity photons and 50% emitters and are well separated from the remaining $N - 1$ dark states whose energies ε_a are within the support of $\rho(\varepsilon)$ and close to the bare energies ω_j. For clarity, the two modes outside the interval $[\omega_{\min}, \omega_{\max}]$ will always be referred to as polaritons throughout the paper, even though this term is usually employed only in the strong-coupling regime in the literature.

Upon coupling to the cavity mode, the ath energy of the dark state ε_a typically gets shifted by an amount of order $1/N$. Defining the energy shift of a dark state $\Delta_a = N[\varepsilon_a - (\omega_{a-1} + \omega_a)/2]$ for energies sorted in increasing order, we determine the value $\overline{\Delta}(\varepsilon)$ of the shift, averaged over a small energy shell $[\varepsilon - \delta\varepsilon/2, \varepsilon + \delta\varepsilon/2]$, to be

$$\overline{\Delta}(\varepsilon) \underset{N\to\infty}{\simeq} \frac{1}{\pi\rho(\varepsilon)} \arctan\left[\frac{\tilde{\rho}(\varepsilon) - \frac{\varepsilon}{\pi g^2}}{\rho(\varepsilon)}\right],$$

where $\tilde{\rho}$ is the Hilbert transform of ρ [see Eqs. (23) and (29)]. This energy shift is closely related to the localization properties of the dark states.

(i) For weak couplings (e.g., for $g/W \ll 1$ for a box distribution of width W), the latter are very close to the bare energy levels, i.e., $\overline{\Delta}(\varepsilon) \approx 1/2\rho(\varepsilon)$. The dark states thus follow the same Poissonian statistics as the independent and identically distributed bare orbitals. The Poisson statistics is a signature of fully localized eigenstates.

(ii) For strong couplings ($g/W \gg 1$), in contrast, the dark states lie roughly at equal distance from the two closest bare energy levels, i.e., $\overline{\Delta}(\varepsilon) \approx 0$, so they follow a statistics that is close to the semi-Poissonian statistics introduced in Ref. [68]. In this regime, the dark states are localized on multiple non-contiguous sites that are close in energy, a behavior referred to as semilocalization [59].

(iii) For intermediate coupling strengths we find that the level spacing statistics depends continuously on g and on the energy ε (see Fig. 8).

2. Inverse participation ratio: Multifractality of the spectrum

In Sec. IV we provide an analytical calculation of the so-called inverse participation ratio (IPR) at large N, which is a useful quantity to characterize the localization properties of the eigenstates [61,69–71]. By computing the scaling behavior of the IPR at large N, we show that all the eigenstates are multifractal for all values of g/W. Multifractality is an extension of the concept of fractal structures of geometric sets, which are characterized by a single fractal dimension, to probability distributions that possess some scale invariance properties and characterized by continuously varying fractal dimensions. We refer the reader to Ref. [72] for a detailed introduction to multifractality. Importantly, the latter is well known to be a meaningful feature of critical wave functions at Anderson transitions [73], with a multifractal spectrum that characterizes the universality class of the transition.

The IPR of the (normalized) eigenstate ψ_a is defined as

$$\mathcal{P}_a(q) = \sum_{j=1}^{N+1} |\psi_{a,j}|^{2q} = \sum_{j=1}^{N} |\langle j, 0\,|\psi_a\rangle|^{2q} + |\langle G, 1\,|\psi_a\rangle|^{2q}. \tag{6}$$

For a delocalized eigenstate, all components are of order $\sim 1/N$ and one expects $\mathcal{P}_a(q) = O(N^{1-q})$. In contrast, for a localized eigenstate, a few components are of $O(1)$ and the others vanish; one thus expects $\mathcal{P}_a(q) = O(1)$. The q-dependent IPR can be viewed as an analog of the Rényi entropy for the probability distribution defined by the squared amplitudes $p_j = |\psi_{a,j}|^2$. For small q, $\mathcal{P}_a(q)$ is sensitive to the tails of that distribution, while for large q it is mostly

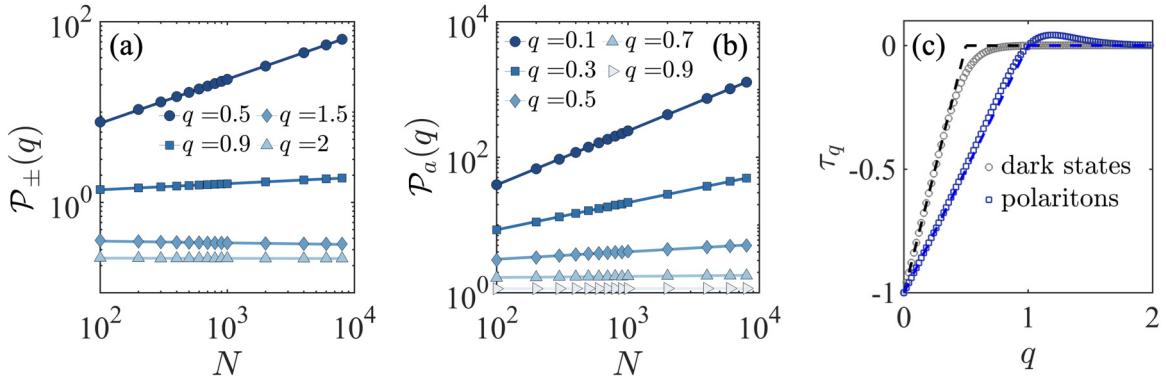

FIG. 3. Scaling behavior of the IPR (see the text) as a function of N for (a) polaritons and (b) dark states. The lines are best fits of the form $aN^{-\tau_q}$. (c) Multifractal exponents τ_q as a function of q for polaritons (blue squares) and dark states (black circles), extracted from the scaling behavior in (a) and (b) for $N = 100$. The analytical results in the thermodynamic limit $N \to \infty$ given by Eq. (7) are shown as dotted lines. The other parameter is $g/W = 2$.

sensitive to the largest components p_j. A qualitative change of the behavior of $\mathcal{P}_a(q)$ as a function of q is a signature of multifractality of the wave function [70,71]. Interestingly, we find that all eigenstates of the TC Hamiltonian (2) exhibit multifractality in that sense.

The scaling behavior of $\mathcal{P}_a(q)$ can be computed analytically at large N. In Sec. IV we show that, remarkably, the $\mathcal{P}_a(q)$ changes as a function of q for all eigenstates of Eq. (2) with the following scalings for the two polaritons and for the $N-1$ dark states, respectively:

$$\mathcal{P}_\pm(q) \underset{N\to\infty}{=} \begin{cases} O(N^{1-q}) & \text{if } q < 1 \\ O(1) & \text{if } q > 1, \end{cases}$$
$$\mathcal{P}_a(q) \underset{N\to\infty}{=} \begin{cases} O(N^{1-2q}) & \text{if } q < \frac{1}{2} \\ O(1) & \text{if } q > \frac{1}{2}. \end{cases} \tag{7}$$

These scaling laws are illustrated in Figs. 3(a) and 3(b), where we show $\mathcal{P}_a(q)$ given by Eq. (6) and computed numerically for finite sizes from the eigenstates (18). For clarity, we display the IPR averaged over the eigenstates: over the two polaritons in Fig. 3(a) and over the $N-1$ dark states in Fig. 3(b). Note that only a single disorder realization is used here since the large fluctuations of $|\psi_{a,j}|^{2q}$ are smoothened by the summation over the eigenstates.

These scalings are valid for all values of $g \neq 0$ and thus demonstrate multifractal behavior of all eigenstates of Eq. (2), for any finite value of the light-matter coupling strength. This is different from conventional disordered hopping models where multifractal behavior is usually associated with the single critical point at a localization-delocalization transition [61].

In order to get a more precise picture of this multifractal behavior, let us imagine that the N spins lie on a d-dimensional lattice of linear size L, then $N \sim L^d$, and the IPR behaves as

$$\mathcal{P}_a(q) \underset{L\to\infty}{\sim} L^{-\tau_q},$$

which defines a set of multifractal exponents τ_q [61]. For the dark states in our model, this standard definition provides

$$\tau_q = \begin{cases} d(2q-1) & \text{if } q < \frac{1}{2} \\ 0 & \text{if } q > \frac{1}{2}. \end{cases} \tag{8}$$

Then, subtracting the part expected for a normal metal where the eigenstates are delocalized, one can define the anomalous dimension $\Delta_q = \tau_q - d(q-1)$ [61]. Usually, in models of Anderson localization-delocalization transitions, this anomalous dimension is expected to satisfy the exact symmetry relation [74]

$$\Delta_q = \Delta_{1-q}. \tag{9}$$

Remarkably, in our random arrowhead matrix model, the exponents (30) for the dark states correspond to the anomalous dimension

$$\Delta_q = d\left(\tfrac{1}{2} - \left|q - \tfrac{1}{2}\right|\right), \tag{10}$$

which does satisfy the symmetry relation (9). On the other hand, for the two polaritons one gets $\Delta_q = \min[0, d(1-q)]$ from Eq. (7), so the symmetry relation is not satisfied by the polariton eigenstates. The multifractal exponents τ_q for polaritons and dark states are computed numerically for $N = 100$ from the scaling of the IPR and shown in Fig. 3(c). We see that finite-size effects are responsible for a smooth crossover between the two regions $q < \frac{1}{2}$ and $q > \frac{1}{2}$ for dark states and $q < 1$ and $q > 1$ for polaritons.

Our analysis suggests that the dark states (and only the dark states) exhibit properties that are analogous to the ones of a multifractal wave function at an Anderson transition. Moreover, the dark-state multifractal spectrum (30) and anomalous dimension (10) turn out to be exactly the same as the ones for the Anderson model on the Bethe lattice [61,75], which is commonly regarded as a mean-field model ($d \to \infty$) of the localization-delocalization transition. Interestingly, the random arrowhead matrix model thus reproduces some aspects of the physics of the Anderson transition in the $d \to \infty$ limit.

3. Photon weight and spectral function

In Sec. V we derive asymptotically exact formulas for the photon weight and the closely related photon spectral function, sometimes referred to as the photon density of states, at large N. The photon weight of an eigenstate ψ_a with energy ε_a is defined as the weight of its $(N+1)$th component, i.e., $\mathcal{W}_a = |\psi_{a,N+1}|^2 \equiv |\langle G, 1|\,|\psi_a\rangle|^2$. It is an important quantity as it allows one to quantify the photon admixture of the

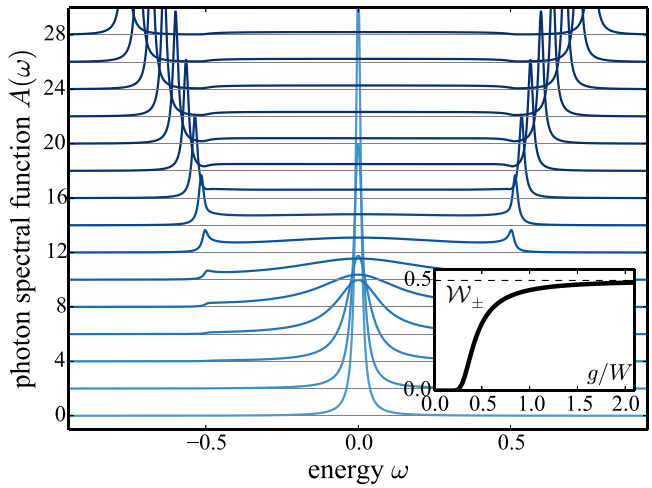

FIG. 4. Photon spectral function $A(\omega)$ given by Eq. (15) for different values of the collective coupling g and for a box disorder distribution of width $W = 1$. From light to dark blue, $g/W = 0$ to $g/W = 0.7$ with 0.05 increments. For readability, each curve is shifted vertically as $A(\omega) \to A(\omega) + 40g$. For the plot we take the convolution of Eq. (15) with a Lorentzian of width $\sigma = 0.01$. The inset shows the photon weight $\mathcal{W}_\pm$ given by Eq. (11) for the box disorder distribution. We see that there are two distinct regimes separated by a smooth crossover: For weak couplings ($g \ll W$) the weight of the two peaks outside the interval $[-W/2, W/2]$ is strongly suppressed, while for strong couplings ($g \gg W$) most of the photon weight is carried by those two peaks, which correspond to polariton modes in that case.

eigenstates and therefore to characterize their hybrid nature (see Fig. 4). The photon weight (or equivalently the photon spectral function) also directly enters the definition of the cavity transmission spectrum [76] and the power spectrum in a resonance fluorescence experiment according to the Wiener-Khinchin theorem [67].

We find that the photon weight of the two polaritons + and − is always of $O(1)$ when $N \to \infty$, as expected, and that it is given by

$$\mathcal{W}_\pm \underset{N\to\infty}{\simeq} \frac{1}{1 - \pi g^2 \tilde{\rho}'(\varepsilon_\pm)} \tag{11}$$

[$\tilde{\rho}'$ denotes the derivative of $\tilde{\rho}$; see Eq. (29)]. In contrast, the photon weight of the dark states is of $O(1/N)$. Its average value over a small energy shell $[\varepsilon - \delta\varepsilon/2, \varepsilon + \delta\varepsilon/2]$ is

$$\overline{\mathcal{W}}(\varepsilon) \underset{N\to\infty}{\simeq} \frac{1}{N} \frac{1/(\pi g)^2}{\rho(\varepsilon)^2 + \left[\tilde{\rho}(\varepsilon) - \frac{\varepsilon}{\pi g^2}\right]^2}. \tag{12}$$

The photon weight per dark state vanishes in the thermodynamic limit, while the photon weight shared by all dark states does not [it remains of $O(1)$] since the number of dark states is $O(N)$. We find that this finite photon weight for $N \to \infty$ is crucial to the existence of semilocalization and cavity-protected transport.

The photon spectral function is defined as the imaginary part of the photon retarded Green's function,

$$A(\varepsilon) = -\frac{1}{\pi} \mathrm{Im}\{[(\varepsilon - H + i0^+)^{-1}]_{N+1,N+1}\}. \tag{13}$$

It is equal to the spectral density, weighted by the photon weights of the eigenstates,

$$A(\varepsilon) = \sum_{a=1}^{N+1} \mathcal{W}_a \delta(\varepsilon - \varepsilon_a). \tag{14}$$

For large N, upon averaging over a small energy shell, the dark-state contribution becomes (for $\varepsilon \in [\omega_{\min}, \omega_{\max}]$)

$$\overline{A}(\varepsilon) \underset{N\to\infty}{\simeq} N\rho(\varepsilon)\overline{\mathcal{W}}(\varepsilon) = \frac{\rho(\varepsilon)/(\pi g)^2}{\rho(\varepsilon)^2 + \left[\tilde{\rho}(\varepsilon) - \frac{\varepsilon}{\pi g^2}\right]^2} \tag{15}$$

All these formulas are exact in the large-N limit. At the leading order in N the spectral function and the photon weight (averaged over an energy shell) take deterministic values: They are self-averaging quantities. The fluctuations of the spectral function $A(\varepsilon)$ around its mean value $\overline{A}(\varepsilon)$ are of $O(1/\sqrt{N})$ in the random arrowhead matrix model. We find that, at this order, the fluctuations of the spectral function $A(\varepsilon)$ around its large-N value $\overline{A}(\varepsilon)$ are Gaussian, characterized by a covariance which we compute exactly [see Eq. (41) for the result and Fig. 11 for an illustration]. Thus, the random arrowhead matrix model allows us to provide analytic expressions for observables, i.e., the mean value and fluctuations of the spectral function $A(\epsilon)$, that are of direct relevance to spectroscopy experiments.

4. Escape probability

In Sec. VI we derive exact asymptotics of all components of the Green's function, or evolution operator $\hat{G}(t) = e^{-i\hat{H}t}$, at the leading order in N. As an application of that result we provide a solution to the following question: What is the probability $P_j(t)$ that an excitation, initially located on site j with energy ω_j, has escaped from this site at time t? This quantity is related to the diffusion properties of excitations throughout the system of emitters. We analyze the behavior of the escape probability $P_j(t) = 1 - |G_{j,j}(t)|^2$ for times t much larger than the width of the distribution $\rho(\omega)$, but also much smaller than $N\rho(\omega)$ (i.e., $1 \ll tW \ll N$ for a box distribution). In that regime we find a diffusivelike behavior $P_j(t) = \Gamma(\omega_j)t$, with an exact formula for the escape rate

$$\Gamma(\omega_j) = 2\pi \left(\frac{g}{\sqrt{N}}\right)^2 \overline{A}(\omega_j), \tag{16}$$

involving the individual coupling strength $g/\sqrt{N}$. We also find that the contribution of dark states to this escape dynamics completely dominates over that of polariton states, consistently with the semilocalization properties of the dark states that are localized on multiple noncontiguous sites. The latter are thus connected to each other via the dark states regardless of the distance separating them, which allows long-range and diffusivelike transfer of excitations throughout the system of emitters.

The resemblance of Eq. (16) to Fermi's golden rule is striking, with the contribution of the dark states to the photon spectral function $\overline{A}(\omega_j)$ [Eq. (15)] playing the role of the photonic density of states. We present an interpretation of this result using an effective Hamiltonian obtained after integrating out the cavity mode in second-order perturbation.

In this effective description the coupling to the cavity provides a long-range hopping term with amplitude depending only on the disordered energies of the emitters, but not on the distance between them. Interestingly, such a diffusive behavior is found for *any* strength of the coupling (in the thermodynamic limit), meaning that arbitrarily small $g/\sqrt{N}$ are sufficient to turn a fully localized phase characterized by the complete absence of diffusion without coupling to the cavity into a new phase with diffusive properties. For any finite coupling strength, we also find that the energy ω_j of the initial site can serve as a knob to control the escape dynamics, which could be exploited in experiments using a narrow-band laser, for instance.

(i) For $\omega_j = 0$, i.e., injection in the middle of the distribution (at resonance with the cavity mode), the escape rate reaches its maximum possible value $2W/\pi N$, independently of g.

(ii) For $\omega_j = \pm W/2$, i.e., injection on the edges of the box distribution, the escape rate vanishes for all values of g.

(iii) In all other cases, the escape rate increases $\sim g^4$ for weak couplings $g \ll W$, reaches its maximum value $2W/\pi N$ for intermediate couplings $g \sim W$, and then saturates to a lower, g-independent value.

This can be understood as the photon weight of the dark states $\mathcal{W}(\omega_j)$ [or equivalently the contribution of the dark states to the photon spectral function $A(\omega_j)$] governing the escape dynamics reaches its maximum value at the center of the distribution and vanishes (logarithmically for a box distribution) at the edges. Surprisingly, we find that the maximum escape rate $2W/\pi N$ increases with the disorder strength, which means that the cavity not only protects transport against disorder but also turns disorder into an ally that can contribute favorably to transport.

Another observable relevant to experiments, using, e.g., a broadband laser, is the disorder-averaged escape rate $\mathbb{E}[\Gamma(\omega_j)]$, which exhibits behavior similar to $\Gamma(\omega_j)$: It grows as g^2 for weak couplings $g \ll W$, reaches a maximum for intermediate couplings $g \sim W$, and then saturates to a lower value for strong couplings $g \gg W$ [Fig. 5(a)]. Moreover, this saturation value is found to grow linearly with W, showing that disorder can help transport also after disorder average, provided coupling is strong enough.

Due to the nonlocal character of the coupling to the cavity, we note that the escape dynamics does not correspond to a standard diffusive motion as the initial excitation does not propagate from one site to the next. A more accurate picture is that the excitation gets *immediately* delocalized over all the emitters, with occupation rising linearly with time, similarly to a diffusive motion.

5. *Out-of-equilibrium transport*

In Sec. VII we investigate out-of-equilibrium transport through the system of emitters in a two-terminal configuration, in relevance to mesoscopic physics [77]. Here two sites (e.g., $j = 1$ and $j = N$) are connected to reservoirs respectively injecting and extracting spin excitations with the rates Γ_{in} and Γ_{out}. We provide analytical expressions for the steady-state excitation current flowing through the system of emitters, which depends on a set of nonequilibrium Green's functions for the emitters and cavity photons, simply connected

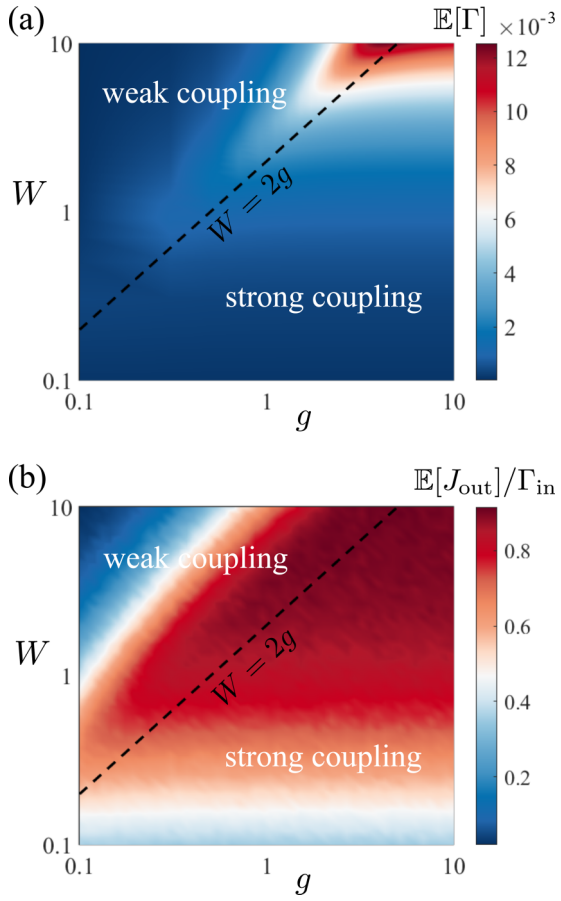

FIG. 5. Cavity-protected transport. (a) Disorder-averaged escape rate $\mathbb{E}[\Gamma]$ and (b) normalized output current $\mathbb{E}[J_{\text{out}}]/\Gamma_{\text{in}}$ as a function of g and W for $N = 500$. The disorder-averaged escape rate is given by Eq. (56), with the photon weights $\mathcal{W}_\pm = |\psi_{\pm,N+1}|^2 = |\langle G, 1|\,|\psi_\pm\rangle|^2$ obtained from the eigenstates (18). The output current given by Eq. (62), with ϵ_a the eigenvalues of the non-Hermitian matrix (17) computed numerically, is averaged over 1000 disorder configurations. The strong- and weak-coupling regimes are separated by the dotted line $W = 2g$, indicating where the energy splitting between the two polaritons precisely equals the width of the disorder distribution. The contribution of the dark states to $\mathbb{E}[J_{\text{out}}]$ is greater than 99%.

to the evolution operator $e^{-i\hat{H}t}$ introduced in Sec. I A 4. The former are conventionally referred to as lesser, $\hat{G}^<(t)$; greater, $\hat{G}^>(t)$; retarded, $\hat{G}^{\text{R}}(t)$; and advanced Green's functions, $\hat{G}^{\text{A}}(t)$, which are all defined in the Appendix. Similar notation is used for the cavity-mode Green's functions. We derive the equations of motion of these Green's functions, assuming that the spin and bosonic operators can all be replaced by fermionic ones. This replacement is valid as long as the system remains in the single-particle sector, which we find to hold when rescaling the current injection rate as $\Gamma_{\text{in}} \to \tilde{\Gamma}_{\text{in}}/N^2$.

Solving the equations of motion allows us to compute the output current $J_{\text{out}} = \Gamma_{\text{out}} n_N$ and the population at each site j,

$$n_j = \int \frac{d\omega}{2\pi} \text{Im}[G^<_{j,j}(\omega)],$$

with $G^<_{j,j}(\omega)$ the Fourier transform of the jth matrix element of the lesser Green's function. We derive analytical formulas for the current and populations, which are found to depend on the eigenvalues of the non-Hermitian arrowhead matrix

$$\left(\begin{array}{ccccc|c} \omega_1 - i\frac{\Gamma_{\text{in}}}{2} & 0 & \cdots & 0 & 0 & g/\sqrt{N} \\ 0 & \omega_2 & \ddots & 0 & 0 & g/\sqrt{N} \\ \vdots & \ddots & \ddots & \ddots & \vdots & \vdots \\ 0 & 0 & \ddots & \omega_{N-1} & 0 & g/\sqrt{N} \\ 0 & 0 & \cdots & 0 & \omega_N - i\frac{\Gamma_{\text{out}}}{2} & g/\sqrt{N} \\ \hline g/\sqrt{N} & g/\sqrt{N} & \cdots & g/\sqrt{N} & g/\sqrt{N} & 0 \end{array}\right). \tag{17}$$

The eigenvalues of this matrix correspond to polaritons and dark states with complex energies due to the in and out couplings to the reservoirs. The latter indeed contribute to the total self-energy through the imaginary numbers $i\Gamma_{\text{in}}/2$ and $i\Gamma_{\text{out}}/2$. This can be interpreted as saying that the eigenstates have acquired a finite lifetime due to the coupling to the environment, which drives the system out of equilibrium.

We find that the disorder-averaged current exhibits behavior similar to the escape rate: It grows as g^2 for weak couplings, reaches a maximum at intermediate couplings $g \sim W$, and then saturates to a lower, g-independent value for strong couplings [Fig. 5(b)]. While for a given $g \ll W$, the current slightly decreases with the disorder strength W, it increases with W for strong enough couplings. This confirms the cavity protection effect observed with the escape dynamics. We also find that the current scales as $\sim 1/N^2$, consistent with the results of Ref. [62]. While this current is equally carried by polaritons and dark states for small N, the contribution of the (broadened) dark states fully dominates in the thermodynamic limit, for all coupling strengths [Fig. 5(c)]. This demonstration of efficient long-range quantum transport is solely mediated by the nonlocal coupling to the cavity and entirely carried by the dark states.

After this summary of our main results, we turn to the detailed analysis of the spectrum and eigenstates of the arrowhead Hamiltonian (2).

II. FINITE SIZE: ENERGY SPECTRUM, EIGENSTATES, AND GREEN'S FUNCTION

We start by recalling some simple exact formulas about arrowhead matrices [6]. For finite N, the eigenstates of the Hamiltonian (2) are, for $1 \leqslant a \leqslant N+1$,

$$H\psi_a = \varepsilon_a \psi_a, \quad \psi_a = N_a \begin{pmatrix} \frac{g/\sqrt{N}}{\varepsilon_a - \omega_1} \\ \frac{g/\sqrt{N}}{\varepsilon_a - \omega_2} \\ \vdots \\ \frac{g/\sqrt{N}}{\varepsilon_a - \omega_N} \\ 1 \end{pmatrix}, \tag{18}$$

with a constant $N_a = (1 + \frac{1}{N}\sum_{j=1}^N \frac{g^2}{(\varepsilon_a - \omega_j)^2})^{-1/2}$ ensuring normalization. The energies ε_a are the solutions of the equation

$$\varepsilon_a = \frac{1}{N}\sum_{j=1}^N \frac{g^2}{\varepsilon_a - \omega_j} \tag{19}$$

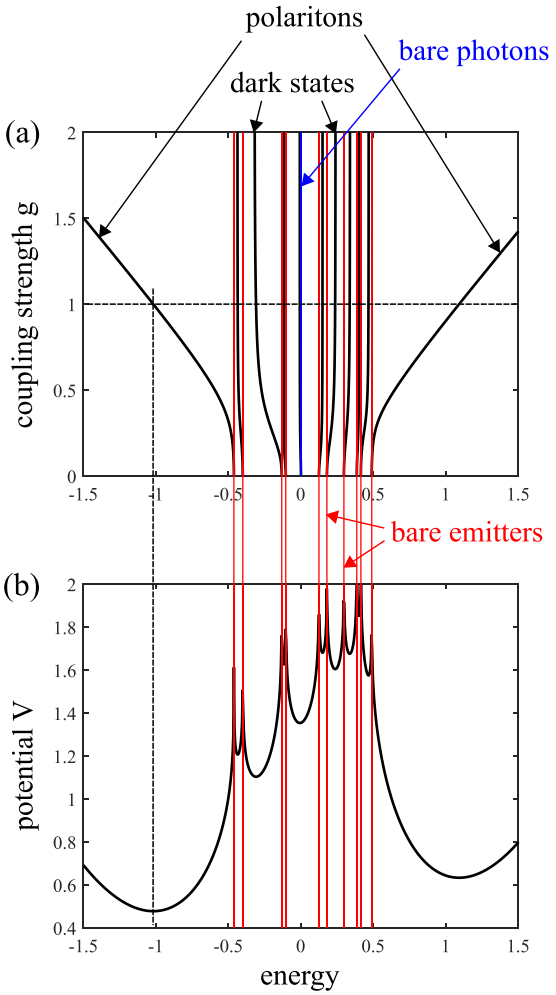

FIG. 6. (a) Energy spectrum (in black) of the Hamiltonian (2) for increasing values of g, here for $N = 10$ emitters with bare energies (in red) drawn from a uniform distribution in the interval $[-\frac{1}{2}, \frac{1}{2}]$ ($W = 1$). The $N-1$ eigenvalues comprised in the interval $[-\frac{1}{2}, \frac{1}{2}]$ are denoted as dark states, while the two unbounded eigenvalues at the edges of the spectrum are referred to as polaritons. The bare photon energy ($\omega = 0$) is depicted in blue. (b) The energy spectrum coincides with the $N+1$ minima of the potential $V(x) = \frac{x^2}{2} - \frac{g^2}{N}\sum_{j=1}^N \log_{10}|x - \omega_j|$, which is plotted with the same bare energies as in (a) and with $g = 1$. There is exactly one minimum between each pair of consecutive bare energies.

and are shown in Fig. 6(a). Note that it is a polynomial equation of degree $N+1$ for ε_a. From now on we work with bare energies ω_j that are sorted in increasing order: $\omega_1 \leqslant \omega_2 \leqslant \cdots \leqslant \omega_N$. Similarly, we label the energies of H in increasing order. Then a very important fact is that the eigenvalues of H are interlaced with the bare energies:

$$\varepsilon_1 \leqslant \omega_1 \leqslant \varepsilon_2 \leqslant \omega_2 \leqslant \cdots \leqslant \omega_{N-1} \leqslant \varepsilon_N \leqslant \omega_N \leqslant \varepsilon_{N+1}. \tag{20}$$

One elementary way of understanding this interlacing is to observe that the ε_a are the $N+1$ minima of the potential $V(x) = \frac{x^2}{2} - \frac{g^2}{N}\sum_{j=1}^N \log_{10}|x - \omega_j|$, which is shown in Fig. 6(b). This potential diverges when $x \to -\infty, \omega_1, \omega_2, \ldots, \omega_N, +\infty$, so it is clear that it possesses

$N+1$ minima which satisfy (20). It is interesting to note that this particular interlacing of the spectrum with the bare energies also appears in other models where long-range interactions generate collective modes on top of a continuum of individual excitations. This occurs, for instance, in an electron gas with Coulomb interactions, where the normal modes are given by the zeros of the dielectric function computed in, e.g. the random-phase approximation [78]. In this case, these normal modes consist of slightly renormalized individual electron-hole excitations across the Fermi surface lying in between the bare individual excitations, as well as a collective unbounded plasmon mode with higher energy. Here the two hybrid light-matter collective states with unbounded energies ε_1 and ε_{N+1} will be referred to as polaritons, while the $N-1$ other individual states with energies ε_j $(j=2,\ldots,N)$ will be referred to as dark states [Fig. 6(a)]. As already mentioned in the Introduction, these dark states exhibit a small but finite photon weight due to the presence of disorder.

In Sec. VI we will be interested in the propagator, or evolution operator, $\hat{G}(t)=e^{-i\hat{H}t}$, which governs the time evolution of the system described by the Hamiltonian (2). The components of this $(N+1)\times(N+1)$ unitary matrix are the Green's functions, which are explicitly defined in the Appendix. One can easily write these Green's functions in closed form using Eq. (18),

$$G_{i,j}(t)=\frac{g^2}{N}\sum_{a=1}^{N+1}\frac{e^{-i\varepsilon_a t}}{(\varepsilon_a-\omega_i)(\varepsilon_a-\omega_j)\big(1+\frac{1}{N}\sum_k\frac{g^2}{(\omega_k-\varepsilon_a)^2}\big)} \tag{21a}$$

for $1\leqslant i,j\leqslant N$,

$$G_{j,N+1}(t)=\frac{g}{\sqrt{N}}\sum_{a=1}^{N+1}\frac{e^{-i\varepsilon_a t}}{(\varepsilon_a-\omega_j)\big(1+\frac{1}{N}\sum_k\frac{g^2}{(\omega_k-\varepsilon_a)^2}\big)} \tag{21b}$$

for $1\leqslant j\leqslant N$, and

$$D(t)\equiv G_{N+1,N+1}(t)=\sum_{a=1}^{N+1}\frac{e^{-i\varepsilon_a t}}{1+\frac{1}{N}\sum_k\frac{g^2}{(\omega_k-\varepsilon_a)^2}}. \tag{21c}$$

Equation (21c) is the photon Green's function, which plays a distinguished role in the analysis of the model and for which we derive the large-N asymptotics in Sec. V. In Sec. VI we derive the large-N asymptotics of the other components (21a) and (21b).

III. SPECTRUM AND MEAN ENERGY SHIFT AT LARGE N

Because of the interlacing (20), it is clear that the vast majority of energies fall in the same interval $[\omega_{\min},\omega_{\max}]$ as the bare energies ω_j. Only the two energy levels ε_1 and ε_{N+1} fall outside that interval. In the thermodynamic limit, the $N-1$ energies $\varepsilon_2,\ldots,\varepsilon_N$ form a continuum of dark states with the same density as the bare energies, i.e., $\sum_{a=2}^{N}\delta(\varepsilon-\varepsilon_a)\simeq N\rho(\varepsilon)$, to leading order in N [see Eq. (3) for the definition of ρ]. The remaining two polariton energy levels are equal to $\varepsilon_1\equiv\varepsilon_-<\omega_{\min}$ and $\varepsilon_{N+1}\equiv\varepsilon_+>\omega_{\max}$, where $\varepsilon_\pm$ are the two solutions of the equation

$$\varepsilon_\pm=\pi g^2\tilde{\rho}(\varepsilon_\pm). \tag{22}$$

Here $\tilde{\rho}$ is the Hilbert transform of ρ,

$$\tilde{\rho}(\varepsilon)=\mathrm{P}\frac{1}{\pi}\int\frac{\rho(\omega)d\omega}{\varepsilon-\omega}, \tag{23}$$

where P stands for the principal value of the integral. Note that the principal value is needed in the definition when the argument ε lies in $[\omega_{\min},\omega_{\max}]$, the support of ρ. Equation (22) is obtained by taking the continuum limit of Eq. (19). In the case of a box distribution for the bare orbitals, i.e., $\rho(\omega)=1/W$ for $\omega\in[-W/2,W/2]$, with $\omega_{\min}=-W/2$ and $\omega_{\max}=W/2$, Eq. (22) becomes

$$\varepsilon_\pm=\pi g^2\frac{1}{\pi W}\log_{10}\left|\frac{\varepsilon_\pm+(W/2)}{\varepsilon_\pm-(W/2)}\right|. \tag{24}$$

For strong couplings $g\gg W$, one recovers $\varepsilon_\pm\simeq\pm g$, i.e., the polariton splitting is roughly twice the collective coupling strength. While the disorder is responsible for an asymmetry between the two polaritons that is clearly seen in Fig. 6(a), it does not lead to important qualitative changes in the polariton spectrum [46], in contrast to dark states.

A more refined description of the spectrum of dark states is obtained as follows. Since the energy ε_a $(2\leqslant a\leqslant N)$ lies in the interval $[\omega_{a-1},\omega_a]$, it is typically at a distance of order $1/N$ from the middle of that interval,

$$\varepsilon_a=\frac{\omega_{a-1}+\omega_a}{2}+\frac{1}{N}\Delta_a\quad\text{for } 2\leqslant a\leqslant N.$$

This defines the shift Δ_a. The shift depends not only on the intensive energy density $\rho(\omega)$ when $N\to\infty$, but also on the microscopic details of the distribution of bare energies. In general, Δ_a is a wildly fluctuating function of its index a and of the bare energies ω_j [see Fig. 7(a)].

By averaging over all eigenstates within a small energy shell $\varepsilon_a\in[\varepsilon-\delta\varepsilon/2,\varepsilon+\delta\varepsilon/2]$, one can define a mean energy shift

$$\overline{\Delta}(\varepsilon)=\frac{1}{N\rho(\varepsilon)\delta\varepsilon}\sum_{|\varepsilon_a-\varepsilon|\leqslant\delta\varepsilon/2}\Delta_a. \tag{25a}$$

For large N, this mean energy shift depends only on the intensive distribution ρ and not on the microscopic details

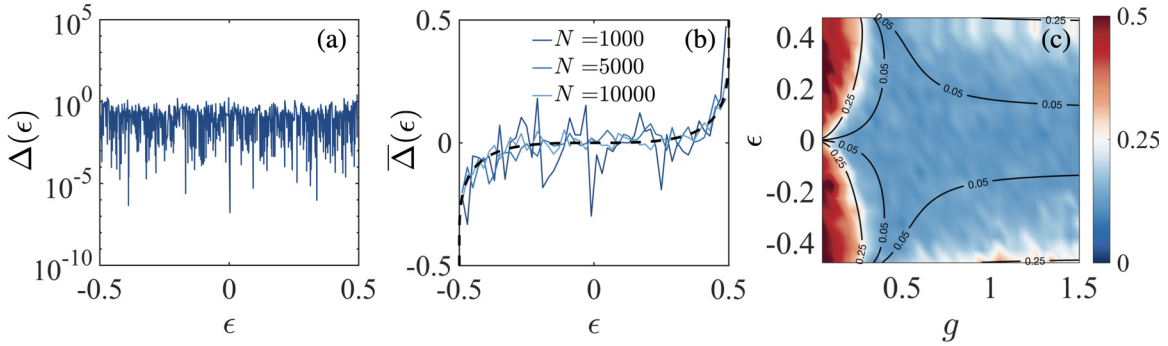

FIG. 7. Energy shift computed numerically from the spectrum of the arrowhead matrix (2) for a given disorder realization, $g = 0.5$, and $W = 1$, (a) without energy binning (average over a small energy shell) for $N = 1000$ and (b) with binning according to Eq. (25a) for different N. (c) Binned energy shift versus energy ε and coupling strength g. The energy shift wildly fluctuates, but its mean value after averaging over a small energy shell converges to the formula (25b) (dotted line) in the thermodynamic limit $N \to \infty$.

or correlations between the bare energies [see Fig. 7(b)]. We find

$$\overline{\Delta}(\varepsilon) \underset{N\to\infty}{=} \frac{1}{\pi\rho(\varepsilon)} \arctan\left[\frac{\tilde{\rho}(\varepsilon) - \frac{\varepsilon}{\pi g^2}}{\rho(\varepsilon)}\right]. \tag{25b}$$

Hence, the spectrum of the $N-1$ dark states has the same distribution as the one of the bare energy levels only at $O(1)$; to $O(1/N)$ the energy levels are pushed by an average amount (25b). As seen in Fig. 7(c), the energy shift averaged over a small energy shell is close to 0.5 for weak couplings $g/W \ll 1$, meaning that the dark states are very close to the bare energy levels. On the other hand, the dark states lie at roughly equal distances from the two closest bare energy levels for strong couplings $g/W \gg 1$, i.e., $\overline{\Delta}(\varepsilon) = 0$.

To arrive at Eq. (25b), one can rely on tricks from complex analysis and contour integration. Let C_a be a counterclockwise contour in the complex plane which encloses the interval $(\varepsilon_a, \omega_a)$ along the real axis. We assume that C_a does not enclose any of the other points $\varepsilon_{a'}$ or $\omega_{a'}$ for $a' \neq a$. Then

$$\oint_{C_a} \frac{dz}{2\pi i} \log_{10}\left(\frac{z-\omega_b}{z-\varepsilon_b}\right) = (\varepsilon_a - \omega_a)\delta_{a,b}.$$

Summing over b from 1 to N and adding the term $\log_{10}[-1/(z-\varepsilon_{N+1})]$ in the sum (for which the contour integral around C_a, $a \leqslant N$, vanishes), one gets

$$\oint_{C_a} \frac{dz}{2\pi i} \log_{10}\left(-\frac{\prod_{b=1}^{N}(z-\omega_b)}{\prod_{c=1}^{N+1}(z-\varepsilon_c)}\right) = \varepsilon_a - \omega_a.$$

The rational function inside the logarithm is nothing but

$$\frac{1}{\frac{1}{N}\sum_{j=1}^{N}\frac{g^2}{z-\omega_j} - z},$$

as can be checked by inspecting the zeros and poles of the latter expression [see Eq. (19)]. For a large number of energy levels ε_a in the small shell $[\varepsilon - \delta\varepsilon/2, \varepsilon + \delta\varepsilon/2]$, one then finds

$$\overline{\Delta}(\varepsilon) \simeq \frac{1}{\rho(\varepsilon)\delta\varepsilon}\left[\frac{\delta\varepsilon}{2} + \sum_{|\varepsilon_a-\varepsilon|\leqslant\delta\varepsilon/2}(\varepsilon_a - \omega_a)\right] = \frac{1}{2\rho(\varepsilon)} + \frac{1}{\rho(\varepsilon)\delta\varepsilon}\sum_{|\varepsilon_a-\varepsilon|\leqslant\delta\varepsilon/2}\oint_{C_a}\frac{dz}{2\pi i}\log_{10}\left(\frac{1}{\frac{1}{N}\sum_j \frac{g^2}{z-\omega_j} - z}\right).$$

We can rewrite this expression as a single contour integral, for a contour $C_{\varepsilon,\delta\varepsilon}$ which encloses all the intervals $(\varepsilon_a, \omega_a)$ in the small energy shell $[\varepsilon - \delta\varepsilon/2, \varepsilon + \delta\varepsilon/2]$. That contour can be deformed close to the real axis, so one can think of it as the union of the two intervals $[\varepsilon - \delta\varepsilon/2, \varepsilon + \delta\varepsilon/2] + i0^+$ and $[\varepsilon - \delta\varepsilon/2, \varepsilon + \delta\varepsilon/2] + i0^-$. Then one takes the $N \to \infty$ limit in the integrand and replaces $\frac{1}{N}\sum_{j=1}^{N}\frac{g^2}{z-\omega_j} - z$ by $\int \frac{g^2\rho(\omega)d\omega}{z-\omega} - z$. This leads to

$$\begin{aligned}
\overline{\Delta}(\varepsilon) &\underset{N\to\infty}{=} \frac{1}{2\rho(\varepsilon)} + \frac{1}{\rho(\varepsilon)\delta\varepsilon}\left(\int_{\varepsilon-\delta\varepsilon/2+i0^-}^{\varepsilon+\delta\varepsilon/2+i0^-} - \int_{\varepsilon-\delta/\varepsilon2+i0^+}^{\varepsilon+\delta\varepsilon/2+i0^+}\right)\frac{dz}{2\pi i}\log_{10}\left(\frac{1}{g^2\int\frac{\rho(\omega)d\omega}{z-\omega} - z}\right) \\
&\simeq \frac{1}{2\rho(\varepsilon)} - \frac{1}{\rho(\varepsilon)}\frac{1}{2\pi i}\left[\log_{10}\left(\int\frac{\rho(\omega)d\omega}{\varepsilon-\omega+i0^-} - \frac{\varepsilon}{g^2}\right) - \log_{10}\left(\int\frac{\rho(\omega)d\omega}{\varepsilon-\omega+i0^+} - \frac{\varepsilon}{g^2}\right)\right] \\
&= \frac{1}{\pi\rho(\varepsilon)}\left\{\frac{\pi}{2} - \frac{1}{2i}\left[\log_{10}\left(i\pi\rho(\varepsilon) + \pi\tilde{\rho}(\varepsilon) - \frac{\varepsilon}{g^2}\right) - \log_{10}\left(-i\pi\rho(\varepsilon) + \pi\tilde{\rho}(\varepsilon) - \frac{\varepsilon}{g^2}\right)\right]\right\} \\
&= \frac{1}{\pi\rho(\varepsilon)}\arg\left[\rho(\varepsilon) + i\left(\tilde{\rho}(\varepsilon) - \frac{\varepsilon}{\pi g^2}\right)\right],
\end{aligned}$$

where we have used the Sokhotski-Plemelj formula. The last line is equivalent to Eq. (25b).

To further characterize the distribution of dark-state energy levels, we investigate the statistics of nearest-neighbor level spacings, within a small energy window $[\varepsilon - \delta\varepsilon/2, \varepsilon + \delta\varepsilon/2]$. In that window we define the normalized spacings as $s_a = N\rho(\epsilon_a)(\varepsilon_{a+1} - \varepsilon_a)$ and we numerically evaluate their probability distribution, by averaging over many disorder realizations, for N large enough so that the energy window contains many levels. We find that the resulting distribution of level spacings when $N \to \infty$ is a one-parameter family of probability distributions $p_\alpha(s)$, parametrized by α, related to the normalized mean energy shift $\rho(\varepsilon)\overline{\Delta}(\varepsilon)$, which itself depends on both the collective coupling g and the energy ε. The parameter α is

$$\alpha = \tan[\pi\rho(\varepsilon)\overline{\Delta}(\varepsilon)] = \frac{\tilde{\rho}(\varepsilon) - \frac{\varepsilon}{\pi g^2}}{\rho(\varepsilon)}.$$

The probability distribution $p_\alpha(s)$ may alternatively be defined as follows, which is more convenient for numerical purposes. Consider N independent and identically distributed variables u_j $(j = 1, \ldots, N)$ drawn from a uniform distribution in [0,1] and the set of N solutions of the equation

$$\alpha + \frac{1}{N}\sum_{j=1}^{N} \frac{1}{\tan[\pi(X - u_j)]} = 0, \quad X \in [0, 1]. \tag{26}$$

One can study the distribution of that set of solutions $\{X_a\}_{1\leqslant a\leqslant N}$ as a function of the parameter α. In particular, ordering the solutions as $0 \leqslant X_1 < X_2 < \cdots < X_N \leqslant 1$ and defining the normalized level spacings as $s_a = N(X_{a+1} - X_a)$ for $a = 1, \ldots, N-1$ and $s_a = N(1 + X_1 - X_N)$ for $a = N$, we can study numerically the distribution of level spacings $p_\alpha(s)$. Note that the level spacing statistics is invariant under the transformation $u_j \to -u_j$ (mod1), $\alpha \to -\alpha$, so we have $p_\alpha(s) = p_{-\alpha}(s)$.

When we replace Eq. (19) by Eq. (26), the idea is that $\pi/\tan[\pi(X_a - u_j)] \sim 1/(X_a - u_j)$, so at small distances the statistics of the roots of both equations must be the same. Moreover, because $1/\tan[\pi(X_a + 1 - u_j)] = 1/\tan[\pi(X_a - u_j)]$, the problem defined by Eq. (26) is the analog of the one defined by Eq. (19), but with periodic boundary conditions. The problem defined in this way is simpler, because it is translation invariant under $u_j \to u_j + U$ mod1 and $X_a \to X_a + U$ mod1 for any U. This is particularly convenient for numerical purposes, because it allows us to study the distribution of energy levels in the entire interval [0,1], without having to restrict to a small energy window as above.

In Fig. 8 we compute the probability distribution $p_\alpha(s)$ numerically by sampling the level spacings between the solutions of Eq. (26), by averaging over 10^4 realizations for $N = 50, 100, 200$. We see in the inset that the results converge quickly to a smooth probability distribution $p_\alpha(s)$ when N increases. The $p_\alpha(s)$ coincides with the Poisson distribution when $\alpha \to \infty$, which simply follows from the fact that $X_j = \omega_j$ in that limit. When $\alpha = 0$, the result is close to a semi-Poisson distribution. For finite values of α the one-parameter family $p_\alpha(s)$ smoothly interpolates between those two limiting distributions.

To summarize, in this section we have characterized the energy spectrum, in particular the spectrum of dark states by computing the average energy shifts (25b) and the statistics

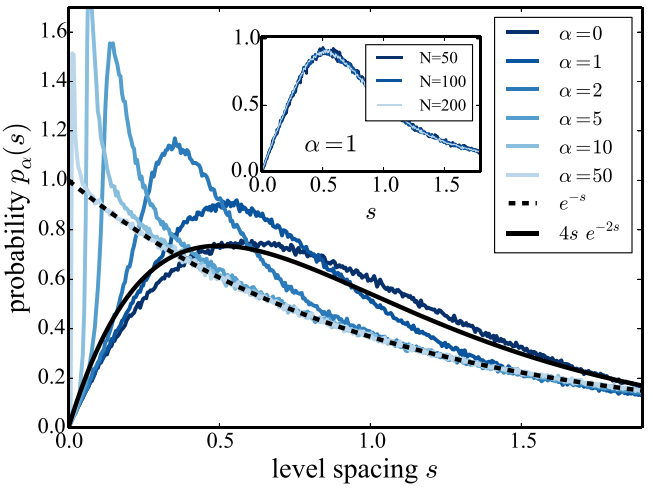

FIG. 8. Probability distribution of level spacings $p_\alpha(s)$ in the model defined by Eq. (26), evaluated numerically for $N = 200$, by averaging over 10^4 independent disorder realizations. Since $p_\alpha(s) = p_{-\alpha(s)}$, we restrict to $\alpha \geqslant 0$. When $\alpha \to \infty$ the distribution is simply the one of independent levels $p_{\text{Poisson}}(s) = e^{-s}$; however, for finite α it is a different distribution which depends continuously on α. When $\alpha = 0$, $p_\alpha(s)$ is close to (but not exactly equal to) the semi-Poisson distribution $p_{\text{semi-Poisson}} = 4se^{-2s}$ of Ref. [68]. The inset shows the same quantity evaluated for $N = 50$, 100, and 200, showing that the results converge as a function N.

of the energy spacings. To compute the energy shifts, note that we have used contour integrals techniques which are sensitive only to the thermodynamic density of states $N\rho(\omega)$, as opposed to higher moments of the disorder distribution. In this paper we will encounter other quantities that share that property and are sensitive only to the density of states, in particular the photon Green's function and the photon spectral function. However, other quantities do depend on the higher moments of the disorder distribution: This is the case for the inverse participation ratio of the eigenstates, which we study in the next section.

IV. INVERSE PARTICIPATION RATIO

In this section we turn to the localization properties of the eigenstates of the arrowhead Hamiltonian (2) and set $g = 1/\sqrt{\pi}$ to lighten our formulas. We study the inverse participation ratio of the eigenstates, which measures their degree of localization and is defined as [see Eq. (18)]

$$\mathcal{P}_a(q) = \sum_{j=1}^{N+1} |\psi_{a,j}|^{2q} = \frac{1 + \frac{1}{(\pi N)^q}\sum_{j=1}^{N} \frac{1}{(\varepsilon_a - \omega_j)^{2q}}}{\left(1 + \frac{1}{\pi N}\sum_{j=1}^{N} \frac{1}{(\varepsilon_a - \omega_j)^2}\right)^q}. \tag{27}$$

A. The IPR of the polaritons

The IPR of the two polaritons behaves as follows when $N \to \infty$:

$$\mathcal{P}_\pm(q) \underset{N\to\infty}{\simeq} \frac{1 + \frac{1}{\pi^q N^{q-1}}\int \frac{\rho(\omega)d\omega}{(\varepsilon_\pm - \omega)^{2q}}}{[1 - \tilde{\rho}'(\varepsilon_\pm)]^q}$$
$$= \begin{cases} N^{1-q}\frac{\frac{1}{\pi^q}\int \frac{\rho(\omega)d\omega}{(\varepsilon_\pm - \omega)^{2q}}}{[1-\tilde{\rho}'(\varepsilon_\pm)]^q} & \text{if } q < 1 \\ \frac{1}{[1-\tilde{\rho}'(\varepsilon_\pm)]^q} & \text{if } q > 1. \end{cases} \tag{28}$$

Here $\tilde{\rho}'(\omega)$ denotes the derivative of $\tilde{\rho}(\omega)$, the Hilbert transform of $\rho(\omega)$. For instance, for a box distribution of width W, i.e., $\rho(\omega) = 1/W$, one has

$$\tilde{\rho}(\omega) = \frac{1}{\pi W} \log_{10} \left| \frac{\omega + (W/2)}{\omega - (W/2)} \right|,$$
$$\tilde{\rho}'(\omega) = \frac{1}{\pi} \frac{1}{(W/2)^2 - \omega^2}. \tag{29}$$

Interestingly, we see that the polariton IPR exhibits a sharp behavior change as a function of q. For $q < 1$, it is of $O(N^{1-q})$, i.e., it grows with N, while it is constant $O(1)$ for $q \geqslant 1$. Assuming that the N spins lie on a d-dimensional lattice of linear size L, the multifractal exponent is defined as

$$\mathcal{P}_a(q) \underset{L\to\infty}{\sim} L^{-\tau_q},$$

which provides

$$\tau_q = \begin{cases} d(q-1) & \text{if } q < 1 \\ 0 & \text{if } q > 1. \end{cases} \tag{30}$$

The polaritons thus behave as metallic (delocalized) states for $q < 1$ and as localized states for $q > 1$, which reflects the fact that polaritons simultaneously share some properties of both localized and delocalized states: They have one component of $O(1)$, like a localized state, and an extensive number of components with weights of $O(1/N)$, like a delocalized state.

B. Scaling of the IPR for the dark states

The IPR of the dark states behaves differently. For eigenenergies ε_a and bare energies ω_a ($2 \leqslant a \leqslant N$) sorted in increasing order, the eigenenergy ε_a lies between ω_{a-1} and ω_a, at a typical distance of $O(1/N)$. Then the scaling of the term $\sum_{j=1}^{N} \frac{1}{(\varepsilon_a - \omega_j)^{2q}}$ is determined as follows. The terms with j such that $|\varepsilon_a - \omega_j| < \delta/N$ for some fixed $\delta > 0$ give a contribution of $O(N^{2q})$, while the contribution of all the other terms can be replaced by the integral $N \int_{|\omega-\varepsilon_a|>\delta/N} \frac{\rho(\omega)d\omega}{(\varepsilon_a-\omega)^{2q}}$, which is of $O(N)$. Thus, the numerator of Eq. (27) is of $O(N^{\max(2q,1)-q})$, while the denominator is of $O(N^q)$. Hence,

$$\mathcal{P}_a(q) = \begin{cases} O(N^{1-2q}) & \text{if } q < \frac{1}{2} \\ O(1) & \text{if } q > \frac{1}{2}. \end{cases}$$

In contrast to conventional disordered hopping models where multifractal behavior is usually associated with the critical point at a localization-delocalization transition [61], we find that multifractality in our model occurs for any strength of the light-matter coupling, thus signaling the existence of a critical phase. On a d-dimensional lattice of size $L \to \infty$, the IPR of the dark states behaves as $\mathcal{P}(q) \sim L^{-\tau_q}$, with

$$\tau_q = \begin{cases} d(2q-1) & \text{if } q < \frac{1}{2} \\ 0 & \text{if } q > \frac{1}{2}. \end{cases}$$

Therefore, the anomalous dimension $\Delta_q = \tau_q - d(q-1)$ for the dark states reads $\Delta_q = d(\frac{1}{2} - |q - \frac{1}{2}|)$, which satisfy the symmetry relation $\Delta_q = \Delta_{1-q}$ like in models of Anderson localization-delocalization transitions [61]. Interestingly, the dark-state anomalous dimension Δ_q turns out to be exactly the same as in the Anderson model on the Bethe lattice [61,75], which is commonly regarded as a mean-field model ($d \to \infty$) of the localization-delocalization transition.

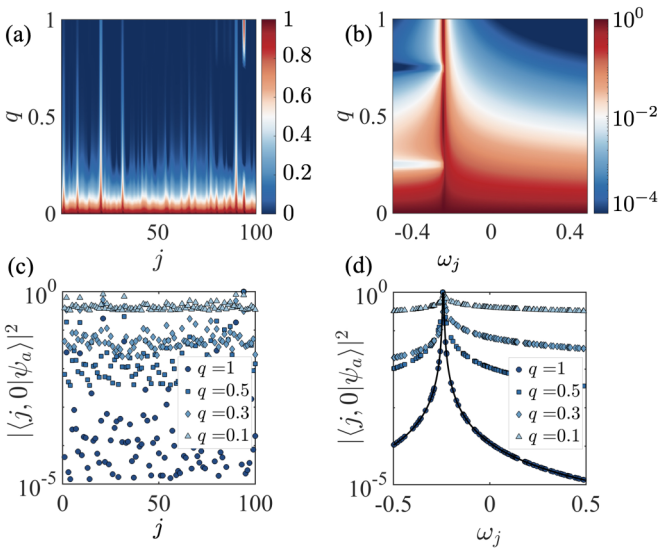

FIG. 9. Multifractality of the dark states. Shown are the components $|\psi_{a,j}|^{2q}$ of $\mathcal{P}_a(q)$ for a given dark state ψ_a with energy $\epsilon_a = -0.24$ (a) as a function of the site position j and (b) sorted according to the energies ω_j of the sites. The fractal structure visible in (a) is caused by the sites random ordering: When the squared amplitudes are sorted according to the energy ω_j, they are a smooth function of ω_j decaying as $\sim 1/(\varepsilon_a - \omega_j)^2$ (see the text). (c) and (d) Display of four cuts ($q = 0.1, 0.3, 0.5, 1$) in (a) and (b), respectively, to better highlight such a power-law decay of the components $|\psi_{a,j}|^{2q}$. The line in (d) for $q = 1$ is a Lorentzian fit.

The multifractality of the spectrum is illustrated in Fig. 9, where the components $|\psi_{a,j}|^{2q}$ of the IPR of the dark states are computed numerically. The multifractal behavior of the dark states arises in an extremely simple way in the random arrowhead matrix model. We find that for independent and identically distributed variables ω_j, the probabilities $p_j = |\psi_{a,j}|^2$ look like a random distribution which exhibits a fractal structure [Figs. 9(a) and 9(c)]. However, when one sorts the amplitudes in order of increasing ω_j, then the probability p_j turns out to be a smooth function of ω_j [Figs. 3(b) and 3(d)]. In fact, it simply decays as a power law,

$$p_j \sim \frac{1}{(\varepsilon_a - \omega_j)^2}. \tag{31}$$

This observation follows directly from the expression of the eigenstates (18) of the matrix (2). It is straightforward to see that the power-law form (31) implies the scaling of the IPR (7) and therefore also the anomalous scaling dimension (10). It is remarkable that the multifractal behavior shown in Fig. 9, which is usually associated with much more complex models in the context of localization-delocalization transitions [61], emerges in such an elementary way in our arrowhead matrix model.

C. An exact formula (not valid for the random disorder distribution)

We have not been able to find a closed analytical formula for the IPR of an eigenstate ψ_a as a function of its energy ε_a, even after averaging over an energy shell $[\varepsilon - \delta\varepsilon/2, \varepsilon + \delta\varepsilon/2]$. In contrast with the energy shift $\Delta(\varepsilon)$ studied in the

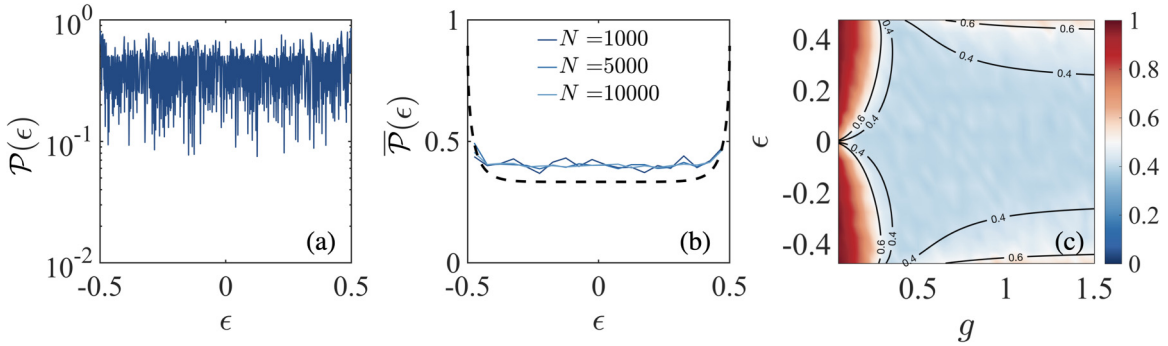

FIG. 10. Inverse participation ratio $\mathcal{P}_a(q=2) \equiv \mathcal{P}(\epsilon)$ of the dark states (ϵ denotes the energies of the eigenstates ϵ_a) computed numerically from Eq. (27) for a given disorder realization, $g = 0.5$, and $W = 1$, (a) without energy binning for $N = 1000$ and (b) with binning for different N. (c) Binned IPR of the dark states versus energy ε and coupling strength g. While the fluctuations of $\overline{\mathcal{P}}$ are reduced as N is increased, the IPR does not converge to the formula (33) obtained for an equally spaced distribution. However, the formula (33) still captures its qualitative behavior as a function of g and ε [contour lines in (c)].

preceding section or with the photon spectral function $A(\varepsilon)$ or the photon weight $\mathcal{W}(\varepsilon)$ studied below, we find that the IPR (27) cannot be expressed in terms of contour integrals that allow us to extract its large-N behavior as a functional of the thermodynamic density of states $N\rho(\omega)$ [see Eq. (3)]. Unlike these quantities, the IPR remains sensitive to the details of the microscopic distribution of bare energies in the large-N limit.

To illustrate this, we have studied the case of a deterministic distribution of bare energies that are locally equally spaced, with thermodynamic density of states $N\rho(\omega)$. Such a distribution is easily constructed as follows: For a given function $\rho(\omega)$, one asks that the bare energies $\omega_1 < \omega_2 < \cdots < \omega_N$ satisfy

$$\omega_{a+1} - \omega_a = \frac{1}{N\rho[(\omega_{a+1} + \omega_a)/2]}. \tag{32}$$

Importantly, this distribution leads to the correct density of states $N\rho(\omega)$ in the thermodynamic limit; however, its correlations between energy levels are clearly very different from the ones obtained from N independent and identically distributed variables as in the random arrowhead Hamiltonian. In particular, independent and identically distributed bare energies would lead to rare pairs of neighboring energies that could be very close to each other, while the equally spaced distribution (32) automatically prevents this and thus exhibits some kind of level repulsion.

For the deterministic equally spaced distribution defined by (32), we have computed the IPR of the dark states ($a = 2, \ldots, N$). Using the fact that

$$\sum_{j=1}^{N} \frac{1}{(\varepsilon_a - \omega_j)^4} \underset{N\gg 1}{\simeq} \frac{\pi^4 N^4}{\rho(\varepsilon_a)^4} \left(\frac{1 - \frac{2}{3}\cos^2[\pi\rho(\varepsilon_a)\Delta(\varepsilon_a)]}{\cos^4[\pi\rho(\varepsilon_a)\Delta(\varepsilon_a)]} \right),$$

we find that the IPR (for $q = 2$) has the large-N asymptotics

$$\mathcal{P}_a(q=2) \underset{N\to\infty}{=} \frac{\frac{\rho(\varepsilon_a)^2}{3} + \left[\tilde{\rho}(\varepsilon_a) - \frac{\varepsilon_a}{\pi g^2}\right]^2}{\rho(\varepsilon_a)^2 + \left[\tilde{\rho}(\varepsilon_a) - \frac{\varepsilon_a}{\pi g^2}\right]^2}. \tag{33}$$

This analytical formula is compared to the numerically evaluated $\mathcal{P}(q=2)$ for the eigenstates of the random arrowhead Hamiltonian in Fig. 10. In Fig. 10(a) we compute $\mathcal{P}_a(q = 2) \equiv \mathcal{P}(\epsilon)$ as a function of ϵ for $N = 1000$ and a single disorder realization, while in Fig. 10(b), $\mathcal{P}(\epsilon)$ is binned into groups of equal energy width and disorder-averaged in each bin for different N. While the fluctuations of the IPR for independent and identically distributed bare energies are reduced upon increasing N, we see that the IPR does not converge to the formula (33) (black dotted line) obtained for the deterministic equally spaced distribution.

This is because, in contrast with the energy shift $\overline{\Delta}(\varepsilon)$ or the photon weight $\overline{\mathcal{W}(\varepsilon)}$, the asymptotic value of the IPR at large N is sensitive not only to the density of states $N\rho(\omega)$, but also remains highly sensitive to the microscopic fluctuations of the bare energy levels.

We note, however, that $\overline{\mathcal{P}}(q=2)$ is well captured qualitatively by the formula (33) [see contour lines in Fig. 10(c)]. For a box disorder distribution of width W and for weak couplings $g/W \ll 1$, the dark states are essentially fully localized with $\overline{\mathcal{P}}(q=2) \approx 1$, except for the states lying in the band center that can always hybridize together via the cavity mode [59]. The dark states thus follow the same Poissonian statistics as the independent and identically distributed bare orbitals. For strong couplings, all dark states can be thought of as semilocalized states, i.e., localized over multiple noncontiguous sites, since they exhibit an intermediate value $\overline{\mathcal{P}}(q=2) \approx 0.4$. The dark states lie roughly at equal distances from the two closest bare energy levels and thus follow a statistics that is close to the semi-Poissonian statistics introduced in Ref. [68]. For intermediate coupling strengths $g \sim W$, the level spacing statistics depends continuously on g and on the energy ε and can therefore be continuously tuned between different statistics.

Now that we have characterized the localization properties of the eigenstates of the Hamiltonian (2) through their inverse participation ratios, we turn to the large-N behavior or the photon Green's function.

V. PHOTON GREEN'S FUNCTION

As hinted in Sec. III, a central role in the analysis of large-N properties of arrowhead Hamiltonians is played by

the photon Green's function in frequency space (see the Appendix),

$$D(z) = \left[\frac{1}{z - H}\right]_{N+1,N+1}.$$

Here $z \in \mathbb{C}$ and, as explained in the Appendix, the limit of $D(z)$ when z approaches a point ω on the real axis from above (below) is the retarded (advanced) Green's function $D^{\mathrm{R}}(\omega) \equiv D(\omega + i0^+)$ [$D^{\mathrm{A}}(\omega \equiv D(\omega + i0^-)$]. To evaluate $D(z)$, one can take the Fourier transform of Eq. (21c), which leads to

$$\begin{aligned} D(z) &= \sum_{a=1}^{N+1} \frac{1}{z - \varepsilon_a} \frac{1}{1 + \frac{1}{\pi N} \sum_{j=1}^{N} \frac{1}{(\varepsilon_a - \omega_j)^2}} \\ &= \frac{1}{z - \frac{1}{\pi N} \sum_{i=1}^{N} \frac{1}{z - \omega_j}} \\ &= \frac{\prod_{j=1}^{N} (z - \omega_j)}{\prod_{a=1}^{N+1} (z - \varepsilon_a)}. \end{aligned} \tag{34}$$

The equalities in the second and third lines are easily checked by inspecting the zeros and poles of these expressions. The result in the third line makes it clear that the function $D(z)$ is very special. It encodes all the spectral properties of our arrowhead Hamiltonian (2): The zeros and poles of $D(z)$ are the bare energies and the eigenvalues of H, respectively.

A. Large-N limit

The large-N limit of $D(z)$ turns out to be an important tool in the analysis of the properties of large arrowhead Hamiltonians. First, we introduce the photon self-energy $\Pi(z) = \frac{1}{\pi N} \sum_{j=1}^{N} \frac{1}{z - \omega_j}$ and its large-N limit

$$\overline{\Pi}(z) = \lim_{N \to \infty} \frac{1}{\pi N} \sum_{j=1}^{N} \frac{1}{z - \omega_j} = \frac{1}{\pi} \int_{\omega_{\min}}^{\omega_{\max}} \frac{\rho(\omega) d\omega}{z - \omega},$$

where $[\omega_{\min}, \omega_{\max}]$ is the support of ρ. Here $\overline{\Pi}(z)$ is analytic in $\mathbb{C} \setminus [\omega_{\min}, \omega_{\max}]$ and it has a discontinuity along that interval: $\overline{\Pi}(\omega + i0^{\pm}) = \tilde{\rho}(\omega) \mp i\rho(\omega)$. Then the large-$N$ limit of the photon Green's function is

$$\overline{D}(z) = \lim_{N \to \infty} D(z) = \frac{1}{z - \overline{\Pi}(z)}.$$

Here $\overline{D}(z)$ has the following properties.

(i) It is analytic in $\mathbb{C} \setminus ([\omega_{\min}, \omega_{\max}] \cup \{\varepsilon_+, \varepsilon_-\})$.

(ii) It has two poles at ε_+ and ε_-: $\overline{D}(z) \underset{z \to \varepsilon_\pm}{\simeq} \frac{1}{[1 - \tilde{\rho}'(\varepsilon_\pm)](z - \varepsilon_\pm)}$.

The residues at these poles are the photon weights of the two polaritons (see next section).

(iii) It has a branch cut along the support of ρ, i.e., $[\omega_{\min}, \omega_{\max}]$. Indeed, for ω along the real axis, $\overline{D}(\omega + i0^{\pm}) = \frac{1}{\omega - \tilde{\rho}(\omega) \pm i\rho(\omega)}$. Thus, $\overline{D}(z)$ has a discontinuity

$$\begin{aligned} \frac{\overline{D}^{\mathrm{A}}(\omega) - \overline{D}^{\mathrm{R}}(\omega)}{2i\pi} &= \frac{\delta(\omega - \varepsilon_+)}{1 - \tilde{\rho}'(\varepsilon_+)} + \frac{\delta(\omega - \varepsilon_-)}{1 - \tilde{\rho}'(\varepsilon_-)} \\ &\quad + \frac{\rho(\omega)/\pi}{\rho(\omega)^2 + (\tilde{\rho}(\omega) - \omega)^2}. \end{aligned} \tag{35}$$

(iv) It behaves as $\overline{D}(z) \simeq \frac{1}{z}$ at infinity.

Below we show how physical quantities such as the photon weight or the photon spectral function are fixed by the analyticity properties of $\overline{D}(z)$, to leading order in N when N is large. Before that, we discuss the fluctuations of $D(z)$ around its asymptotic value $\overline{D}(z)$.

B. Fluctuations of the photon Green's function

When the bare energies ω_j are independent and identically distributed random variables, the function $D(z)$ also has a nondeterministic subleading part. Our goal is to characterize the fluctuations of $D(z)$ around its mean value. Let us start by introducing the random function

$$\phi(z) = \sqrt{N} \left(\frac{1}{\pi N} \sum_{j=1}^{N} \frac{1}{z - \omega_j} - \overline{\Pi}(z) \right) \tag{36}$$

which measures the fluctuations of the photon self-energy $\Pi(z)$ around its large-N limit. Note that $\phi(z)$ has zero mean value for the disorder average (4),

$$\mathbb{E}[\phi(z)] = 0.$$

The factor $\sqrt{N}$ in Eq. (36) is introduced such that the covariance of $\phi(z)$ is of order one:

$$\begin{aligned} \mathrm{cov}[\phi(z_1)\phi(z_2)] &= \mathbb{E}[\phi(z_1)\phi(z_2)] \\ &= \frac{1}{N} \sum_{i,j} \mathbb{E}\left[\left(\frac{1}{\pi} \frac{1}{z_1 - \omega_i} - \overline{\Pi}(z_1) \right) \right. \\ &\qquad \left. \times \left(\frac{1}{\pi} \frac{1}{z_2 - \omega_j} - \overline{\Pi}(z_2) \right) \right] \\ &= \frac{1}{\pi^2 N} \sum_{j=1}^{N} \mathbb{E}\left[\frac{1}{z_1 - \omega_j} \frac{1}{z_2 - \omega_j} \right] \\ &\quad - \overline{\Pi}(z_1)\overline{\Pi}(z_2) \\ &= \frac{1}{\pi^2} \int \frac{\rho(\omega) d\omega}{(z_1 - \omega)(z_2 - \omega)} - \overline{\Pi}(z_1)\overline{\Pi}(z_2) \\ &= -\frac{\overline{\Pi}(z_1) - \overline{\Pi}(z_2)}{\pi(z_1 - z_2)} - \overline{\Pi}(z_1)\overline{\Pi}(z_2). \end{aligned} \tag{37}$$

More generally, the connected part of the pth-order correlation of $\phi(z)$ scales as $\sim N^{-p/2}$, so at large N it vanishes for all $p \geqslant 3$,

$$\mathbb{E}[\phi(z_1)\phi(z_2) \cdots \phi(z_p)]_{\mathrm{conn}} \underset{N \to \infty}{\longrightarrow} 0 \quad \text{if } p \geqslant 3.$$

Thus, the random function $\phi(z)$ is Gaussian, with mean value zero and covariance (37). The fluctuations of the photon Green's function are then obtained as

$$\begin{aligned} D(z) &= \frac{1}{z - \overline{\Pi}(z) - \frac{1}{\sqrt{N}}\phi(z)} \\ &= \frac{1}{z - \overline{\Pi}(z)} + \frac{1}{[z - \overline{\Pi}(z)]^2} \frac{1}{\sqrt{N}} \phi(z) + \cdots \\ &= \overline{D}(z) + \frac{1}{\sqrt{N}} \overline{D}^2(z)\phi(z) + O\left(\frac{1}{N}\right). \end{aligned} \tag{38}$$

Thus, the fluctuations of $D(z)$ around its large-N value $\overline{D}(z)$ are also Gaussian and of order $1/\sqrt{N}$ and they are directly determined by the two-point function (37).

C. Photon spectral function: Mean value and fluctuation statistics

The photon spectral function is proportional to the cavity transmission and fluorescence emission spectra, which can be directly accessed by, e.g., Fourier transform spectroscopy [67,76]. It is obtained from the imaginary part of the retarded Green's function (see the Appendix),

$$A(\omega) = -\frac{1}{2i\pi}[D^{\mathrm{R}}(\omega) - D^{\mathrm{A}}(\omega)] = -\frac{1}{\pi}\mathrm{Im}D^{\mathrm{R}}(\omega). \quad (39)$$

In the large-N limit this is equal to [using the poles of the function $\overline{D}(z)$ and Eq. (35)]

$$\overline{A}(\omega) \underset{N\to\infty}{\simeq} \frac{\delta(\omega-\varepsilon_+)}{1-\tilde{\rho}'(\varepsilon_+)} + \frac{\delta(\omega-\varepsilon_-)}{1-\tilde{\rho}'(\varepsilon_-)} + \frac{\rho(\omega)/\pi}{\rho(\omega)^2+[\tilde{\rho}(\omega)-\omega]^2}. \quad (40)$$

Note that the spectral function should satisfy the sum rule $\int A(\omega)d\omega = 1$, which is a consequence of Eq. (14) and of the normalization of the eigenstates. The fact that the sum rule is satisfied by (40) follows from contour integration. Integrating the function $\overline{D}(z)$ along a counterclockwise contour C that encloses both the interval $[\omega_{\min}, \omega_{\max}]$ and the two points $\varepsilon_\pm$, one gets $\frac{1}{2\pi i}\oint_C \overline{D}(z)dz = \int \overline{A}(\omega)d\omega$. The contour C can then be deformed to infinity, and one concludes that $\frac{1}{2\pi i}\oint_C \overline{D}(z)dz = 1$ using the above property (iv) of the function $\overline{D}(z)$.

With the formalism of the preceding section, we can go beyond the leading order (40) and calculate the $O(1/\sqrt{N})$ fluctuations of $A(\omega)$ around its mean value $\mathbb{E}[A(\omega)] = \overline{A}(\omega)$. Combining Eqs. (39) and (38), one sees that the connected correlations of $A(\omega)$ can be expressed in terms of those of $\phi(\omega)$. In particular, the covariance of $A(\omega)$ can be expressed in terms of the known covariance of $\phi(\omega)$ through

$$\begin{aligned}
\mathrm{cov}[A(\omega_1), A(\omega_2)] &\equiv \mathbb{E}[A(\omega_1)A(\omega_2)] - \mathbb{E}[A(\omega_1)]\mathbb{E}[A(\omega_2)] \\
&= \frac{-1}{(2\pi)^2}\mathrm{cov}[D^{\mathrm{R}}(\omega_1) - D^{\mathrm{A}}(\omega_1), D^{\mathrm{R}}(\omega_2) - D^{\mathrm{A}}(\omega_2)] \\
&= \frac{-1}{(2\pi)^2}\frac{1}{N}\{[\overline{D}^{\mathrm{R}}(\omega_1)]^2[\overline{D}^{\mathrm{R}}(\omega_2)]^2\mathrm{cov}[\phi^{\mathrm{R}}(\omega_1), \phi^{\mathrm{R}}(\omega_2)] \\
&\quad - [\overline{D}^{\mathrm{A}}(\omega_1)]^2[\overline{D}^{\mathrm{R}}(\omega_2)]^2\mathrm{cov}[\phi^{\mathrm{A}}(\omega_1), \phi^{\mathrm{R}}(\omega_2)] \\
&\quad - [\overline{D}^{\mathrm{R}}(\omega_1)]^2[\overline{D}^{\mathrm{A}}(\omega_2)]^2\mathrm{cov}[\phi^{\mathrm{R}}(\omega_1), \phi^{\mathrm{A}}(\omega_2)] \\
&\quad + [\overline{D}^{\mathrm{A}}(\omega_1)]^2[\overline{D}^{\mathrm{A}}(\omega_2)]^2\mathrm{cov}[\phi^{\mathrm{A}}(\omega_1), \phi^{\mathrm{A}}(\omega_2)]\} \\
&\quad + O(N^{-3/2}).
\end{aligned}$$

Using the result (37), the Sokhotski-Plemelj formula, and combining all the terms, one arrives at the result for the covariance of the photon spectral function for $\omega_1, \omega_2 \in [\omega_{\min}, \omega_{\max}]$,

$$\frac{\mathrm{cov}[A(\omega_1), A(\omega_2)]}{\mathbb{E}[A(\omega_1)]\mathbb{E}[A(\omega_2)]} = \frac{1}{N\rho(\omega_1)}\delta(\omega_1-\omega_2) + \frac{1}{N}\frac{\frac{2}{\pi}\frac{(\omega_2-\tilde{\rho}_2)(\rho_1^2+\tilde{\rho}_1^2-\omega_1^2)-(\omega_1-\tilde{\rho}_1)(\rho_2^2+\tilde{\rho}_2^2-\omega_2^2)}{\omega_1-\omega_2} - \left(\rho_1^2+\tilde{\rho}_1^2-\omega_1^2\right)\left(\rho_2^2+\tilde{\rho}_2^2-\omega_2^2\right)}{[\rho_1^2+(\tilde{\rho}_1-\omega_1)^2]\left[\rho_2^2+(\tilde{\rho}_2-\omega_2)^2\right]} + O(N^{-3/2}), \quad (41)$$

with $\rho_{1,2} = \rho(\omega_{1,2})$ and $\tilde{\rho}_{1,2} = \tilde{\rho}(\omega_{1,2})$.

Equation (41) entirely characterizes the fluctuations of the photon spectral function around its mean value (40), at $O(1/N)$. The non-Gaussianity of the fluctuations appears only at higher order. In Fig. 11 we display typical results for $A(\omega)$ for different disorder realizations: The fluctuations around the mean value $\overline{A}(\omega)$ is clearly visible [see the inset of Fig. 11(a)]. We also display the numerical estimate of the covariance $\mathrm{cov}[A(\omega_1), A(\omega_2)]$, obtained by averaging over 1000 disorder realizations for a system size $N = 50$ [see Fig. 11(b)]; the result matches Eq. (41), as expected. We note that the covariance carries distinct features for weak and strong couplings. In the latter case, deviations with respect to the mean value of the spectral function are correlated (same sign) only along the diagonal $\epsilon_1 = \epsilon_2$ [Fig. 11(b)]. For weak couplings, however, there are other regions where both correlations and anticorrelations (opposite sign) are observed.

Now that we have characterized the large-N behavior of the photon spectral function $A(\omega)$, including its fluctuations, we turn to the closely related photon weight.

D. Photon weights

The photon weight of an eigenstate ψ_a with energy ε_a is defined as the weight of its $(N+1)$th component [see Eq. (18)], i.e., $\mathcal{W}_a = |\psi_{a,N+1}|^2 \equiv |\langle G, 1|\psi_a\rangle|^2$. Using the definitions of Sec. V, one can easily see that the photon weight precisely corresponds to the quasiparticle weight of the eigenstates

$$A(\varepsilon) = \sum_{a=1}^{N+1} \mathcal{W}_a \delta(\varepsilon - \varepsilon_a). \quad (42)$$

The photon weight of the two polaritons $+$ and $-$ is directly obtained from Eq. (40) and reads

$$\mathcal{W}_\pm \underset{N\to\infty}{\simeq} \frac{1}{1-\tilde{\rho}'(\varepsilon_\pm)}.$$

It is of $O(1)$ (i.e., independent of N) in the thermodynamic limit and goes asymptotically to $\frac{1}{2}$ for $g \to \infty$. For instance, for a flat disorder distribution in the interval $[-W/2, W/2]$,

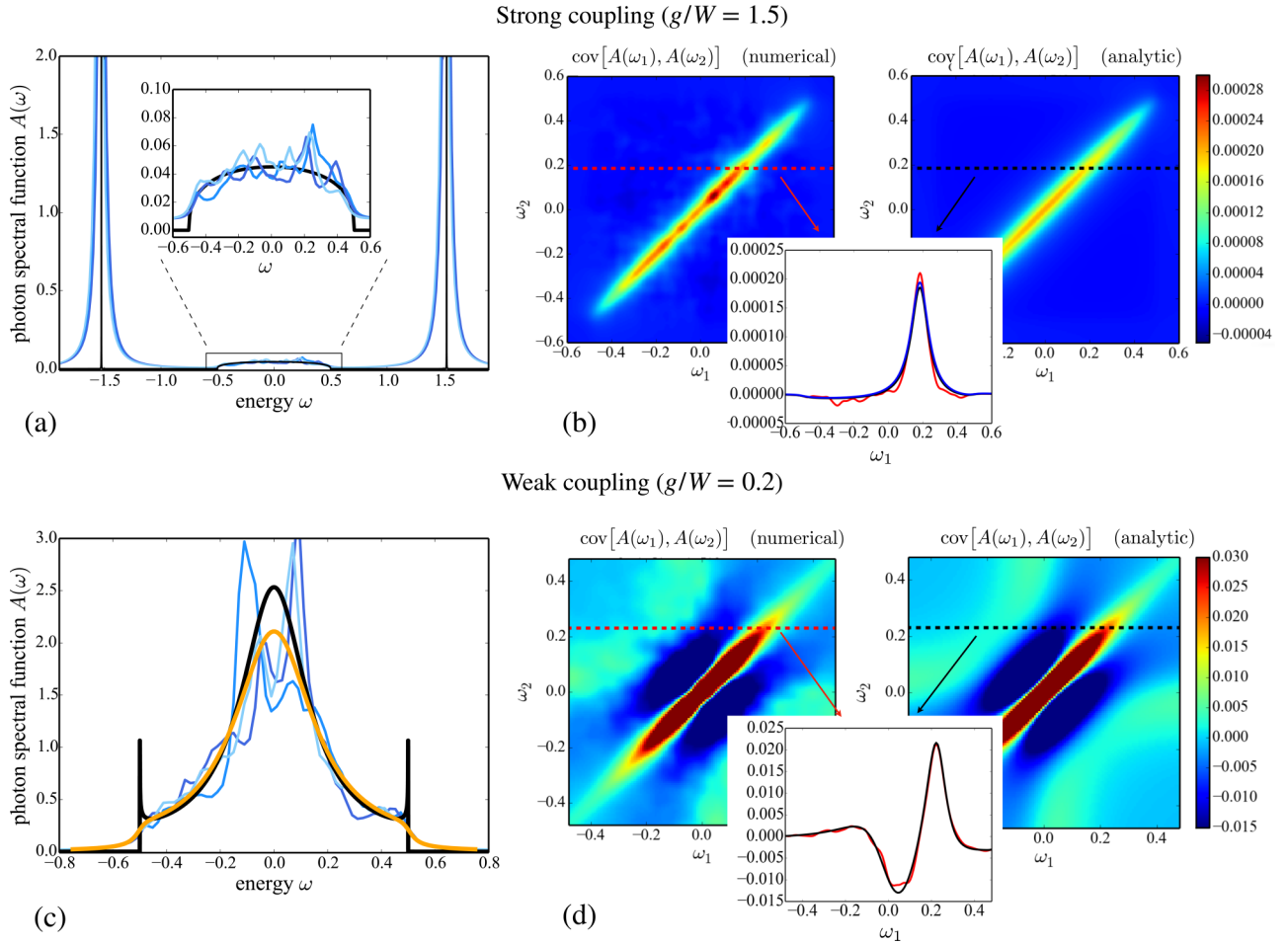

FIG. 11. (a) Photon spectral function $A(\omega)$ for $g = 1.5$, $W = 1$, and $N = 100$, for three different disorder configurations (blue curves), compared to the analytical formula (40) valid in the thermodynamic limit (black curve); $A(\omega)$ is computed using Eq. (42), where the Dirac delta $\delta(\omega - \varepsilon_a)$ is replaced by the Lorentzian $\sigma/\pi/[(\omega - \varepsilon_a)^2 + \sigma^2]$ of width $\sigma = 0.03$. We clearly see the two large peaks at the lower and upper polariton energies $\varepsilon_\pm$ [see Eq. (40)]. Here $A(\omega)$ is displayed for three different disorder realizations (blue curves). The inset is a close-up of the window $\omega \in [\omega_{\min}, \omega_{\max}] = [-W/2, W/2]$: We see that the spectral function fluctuates around its mean value $\overline{A}(\omega)$ given by Eq. (40), drawn in black. In the text, we show that the fluctuations of $A(\omega)$ around its mean value are of $O(1/\sqrt{N})$ and that they are Gaussian at that order. (b) Numerical evaluation of the covariance $\mathrm{cov}[A(\omega_1), A(\omega_2)]$ and comparison with the analytic formula (41). The numerical estimate of the covariance is obtained by averaging over 1000 independent disorder realizations. Both the numerical and the analytic curves include a convolution with the Lorentzian of width $\sigma = 0.03$. (c) Same as in (a), with $g = 0.2$ (and $W = 1$, $N = 100$, and $\sigma = 0.03$). The three blue curves are typical results for different disorder realizations. The black line is the analytic formula (40) and the orange line is its convolution with the Lorentzian of width $\sigma = 0.03$. (d) Same as in (b), for $g = 0.2$.

one finds $\mathcal{W}_\pm \approx \frac{1}{2} - \frac{W^2}{24g^2}$ for $g/W \gg 1$. In this regime, the polaritons are collective light-matter states, half composed of the N excited emitters [each with a weight $O(1/N)$] and the photon. Instead, for weak coupling, polaritons lose their collective nature. For a flat disorder distribution, one can show using Eq. (24) that, for $g/W \ll 1$,

$$\mathcal{W}_\pm \underset{N\to\infty}{\simeq} \left(\frac{W}{g}\right)^2 e^{-W^2/2g^2} \underset{g/W\to 0}{\to} 0.$$

The photon weight of the dark states ($2 \leqslant a \leqslant N$) is more complicated. Like the mean energy shift, it fluctuates wildly as a function of the index a and of the bare energy levels. However, its average value over eigenstates within a small energy shell $[\varepsilon - \delta\varepsilon/2, \varepsilon + \delta\varepsilon/2]$,

$$\overline{\mathcal{W}}(\varepsilon) = \frac{1}{N\rho(\epsilon)\delta\varepsilon} \sum_{|\varepsilon_a - \varepsilon| \leqslant \delta\varepsilon/2} \mathcal{W}_a, \tag{43}$$

is independent of the microscopic details of the distribution of bare energies and takes a simple form in the limit $N \to \infty$. Using Eqs. (40) and (42), we find that

$$\overline{A}(\varepsilon) \underset{N\to\infty}{\simeq} N\rho(\varepsilon)\overline{\mathcal{W}}(\varepsilon),$$

with

$$\overline{\mathcal{W}}(\varepsilon) = \frac{1}{N} \frac{1/\pi}{\rho(\varepsilon)^2 + [\tilde{\rho}(\varepsilon) - \varepsilon]^2}. \tag{44}$$

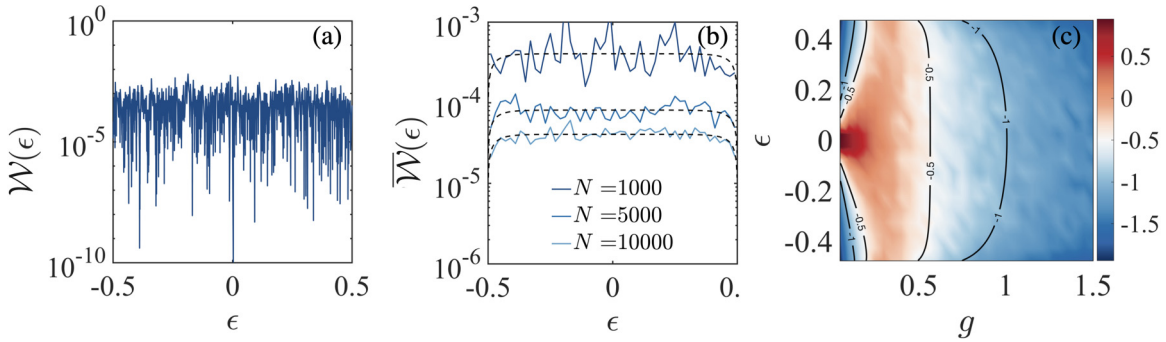

FIG. 12. Photon weight of the dark states computed numerically from the eigenvectors (18) for a given disorder realization, $g = 0.5$ and $W = 1$, (a) without energy binning for $N = 1000$ and (b) with binning according to Eq. (43) for different N. (c) Binned photon weight of the dark states versus energy ε and coupling strength g. The color bar is in logarithmic scale. Similarly to the energy shift, the photon weight wildly fluctuates but its mean value after averaging over a small energy shell converges to the formula (44) (dotted lines) in the thermodynamic limit $N \to \infty$.

Thus, one finds that the photon weight of the dark states, which is inherited from the indirect coupling between these dark states and the cavity mode in the presence of disorder, is of $O(1/N)$. It is interesting to note that for a finite but arbitrarily small g/W, the photon weight of the polaritons saturates to a finite value as N grows, which results in the photon weight being mostly concentrated on the two polaritons even for weak couplings, provided N is large enough.

The photon weight of the dark states is plotted in Fig. 12. For a given disorder realization, one finds that $\mathcal{W}(\varepsilon)$ wildly fluctuates in the large-N limit [Fig. 12(a)], while the amplitude of fluctuations is reduced upon averaging over a small energy shell (energy binning). Upon increasing N, the binned photon weight $\overline{\mathcal{W}}(\varepsilon)$ converges to the exact formula (44) [Fig. 12(b)]. While being nonzero only at the cavity energy $\varepsilon = 0$ for $g = 0$, the binned photon weight is spread over the dark states as g is increased for a fixed N. For strong couplings $g \gg W$, the photon weight is mostly concentrated in the two polariton states, while the dark states retain a photon weight $\sim O(1/N)$.

VI. REAL-TIME GREEN'S FUNCTIONS AT LARGE N AND APPLICATION TO THE ESCAPE PROBABILITY

So far we have analyzed the model defined by the arrowhead Hamiltonian (2) from the point of view of its spectral properties: We have focused on its spectrum composed of two polariton modes and of a continuum of dark states in the $N \to \infty$ limit and on the photon Green's function in frequency space, closely related to the photon spectral function and to the photon weights of the eigenstates. In this section we turn to the real-time dynamics of the model. We first compute the real-time Green's functions in the large-N limit and provide explicit formulas for those. We then exploit these exact results to analyze the probability that an excitation initially located on site j has escaped from that site after time t. We interpret our result for the escape rate in terms of Fermi's golden rule in an effective model, where the cavity mode has been integrated out in second-order perturbation. We demonstrate the existence of a diffusive dynamics solely mediated by the coupling to the cavity and a cavity-protection effect for strong enough couplings, where transport properties are enhanced with increasing disorder. Cavity-enhanced out-of-equilibrium transport occurring when coupling the system of emitters to two external leads is investigated in the next section.

A. Large-N asymptotics of the real-time Green's functions

Here we return to the real-time Green's functions (21a)–(21c) and analyze their large-N asymptotics. We start with the photon Green's function: In real time, we have [see Eq. (21), with our convention $\pi g^2 = 1$]

$$D(t) \equiv G_{N+1,N+1}(t) = \sum_{a=1}^{N+1} \frac{e^{-i\varepsilon_a t}}{1 + \frac{1}{\pi N}\sum_k \frac{1}{(\omega_k - \varepsilon_a)^2}} = \oint_C \frac{dz}{2\pi i} e^{-izt} D(z),$$

where $D(z)$ is given in (34) and the counterclockwise contour C encloses all the eigenvalues of H. To take the large-N limit, we can replace $D(z)$ by $\overline{D}(z)$ and evaluate the contour integral using the analyticity properties of $\overline{D}(z)$ [see Sec. V and in particular Eq. (35)]. This gives

$$G_{N+1,N+1}(t) \underset{N\to\infty}{=} \frac{e^{-i\varepsilon_+ t}}{1 - \tilde{\rho}'(\varepsilon_+)} + \frac{e^{-i\varepsilon_- t}}{1 - \tilde{\rho}'(\varepsilon_-)} + \frac{1}{\pi}\int \frac{e^{-i\omega t}\rho(\omega) d\omega}{\rho(\omega)^2 + [\tilde{\rho}(\omega) - \omega]^2}.$$

Importantly, that result does not depend of the microscopic details of the distribution of bare energies. The real-time photon Green's function is not sensitive to fluctuations of that distribution in the large-N limit; in other words, the real-time Green's function is sensitive only to the average density of states $N\rho(\omega)$ [Eq. (3)].

The other Green's functions (21a) and (21b) share that property and they can be obtained in a similar way. For the

component $G_{j,N+1}(t)$ $(1 \leqslant j \leqslant N)$ we find

$$\begin{aligned} G_{j,N+1}(t) &= \frac{1}{\sqrt{\pi N}} \sum_{a=1}^{N+1} \frac{e^{-i\varepsilon_a t}}{(\varepsilon_a - \omega_j)\big(1 + \frac{1}{\pi N}\sum_{k=1}^{N} \frac{1}{(\omega_k - \varepsilon_a)^2}\big)} = \frac{1}{\sqrt{\pi N}} \oint_C \frac{dz}{2\pi i} \frac{e^{-izt}}{z - \omega_j} D(z) \\ &\underset{N\to\infty}{=} \frac{1}{\sqrt{\pi N}} \Bigg[\frac{e^{-i\varepsilon_+ t}}{(\varepsilon_+ - \omega_j)[1 - \tilde{\rho}'(\varepsilon_+)]} + \frac{e^{-i\varepsilon_- t}}{(\varepsilon_- - \omega_j)[1 - \tilde{\rho}'(\varepsilon_-)]} \\ &\qquad + \mathrm{P}\frac{1}{\pi} \int \frac{e^{-i\omega t} \rho(\omega) d\omega}{(\omega - \omega_j)\{\rho(\omega)^2 + [\tilde{\rho}(\omega) - \omega]^2\}} + \frac{1}{\pi} \frac{e^{-i\omega_j t}[\tilde{\rho}(\omega_j) - \omega_j]}{\rho(\omega_j)^2 + [\tilde{\rho}(\omega_j) - \omega_j]^2} \Bigg], \end{aligned}$$

where P denotes the Cauchy principal value of the integral. The large-N asymptotics of $G_{i,j}(t)$ with $1 \leqslant i \neq j \leqslant N$ also follows from that result, because

$$G_{i,j}(t) = \frac{1}{\pi N} \sum_{a=1}^{N+1} \frac{e^{-i\varepsilon_a t}}{(\varepsilon_a - \omega_i)(\varepsilon_a - \omega_j)\big(1 + \frac{1}{\pi N}\sum_{k=1}^{N} \frac{1}{(\omega_k - \varepsilon_a)^2}\big)} = -\frac{1}{\sqrt{\pi N}} \frac{G_{i,N+1}(t) - G_{j,N+1}(t)}{\omega_i - \omega_j}.$$

Finally, for $1 \leqslant j \leqslant N$ we find

$$\begin{aligned} G_{j,j}(t) &= \frac{1}{\pi N} \sum_{a=1}^{N+1} \frac{e^{-i\varepsilon_a t}}{(\varepsilon_a - \omega_j)^2\big(1 + \frac{1}{\pi N}\sum_{k=1}^{N} \frac{1}{(\omega_k - \varepsilon_a)^2}\big)} = \oint_C \frac{dz}{2\pi i} \frac{e^{-izt}}{(z - \omega_j)^2} \left[(z - \omega_j) + \frac{D(z)}{\pi N} \right] \\ &\underset{N\to\infty}{=} e^{-i\omega_j t} + \frac{1}{\pi N} \Bigg\{ \frac{e^{-i\varepsilon_+ t}}{(\varepsilon_+ - \omega_j)^2[1 - \tilde{\rho}'(\varepsilon_+)]} + \frac{e^{-i\varepsilon_- t}}{(\varepsilon_- - \omega_j)^2[1 - \tilde{\rho}'(\varepsilon_-)]} + it \frac{e^{-i\omega_j t}[\tilde{\rho}(\omega_j) - \omega_j]}{\rho(\omega_j)^2 + [\tilde{\rho}(\omega_j) - \omega_j]^2} \\ &\qquad + F\frac{1}{\pi} \int \frac{e^{-i\omega t} \rho(\omega) d\omega}{(\omega - \omega_j)^2\{\rho(\omega)^2 + [\tilde{\rho}(\omega) - \omega]^2\}} + e^{-i\omega_j t} \partial_{\omega_j} \left(\frac{\tilde{\rho}(\omega_j) - \omega_j}{\rho(\omega_j)^2 + [\tilde{\rho}(\omega_j) - \omega_j]^2} \right) \Bigg\}, \end{aligned} \tag{45}$$

where F stands for the Hadamard finite part of the integral. We now turn to a concrete example to illustrate how such formulas can be exploited, by evaluating the probability that an excitation, located on site j at time $t = 0$, is found elsewhere at time $t > 0$.

B. Application to the escape probability

As a simple application of the above results for the real-time Green's functions, we study the probability that an excitation, initially on a given site j $(j = 1, \ldots, N)$, has escaped from this site at time t:

$$P_j(t) = 1 - |G_{j,j}(t)|^2. \tag{46}$$

We are mostly interested in the behavior of $P_j(t)$ at large time $t \gg \rho(\omega)$, but not too large so that the continuum limit still holds, i.e., $t \ll N\rho(\omega)$. So we take the $N \to \infty$ limit first and then consider large time t. The $N \to \infty$ limit of $G_{j,j}(t)$ is given by Eq. (45), so we need to analyze the large-t behavior of that expression.

The right-hand side of Eq. (45) is a sum of six terms; of all these terms, four are clearly bounded as a function of t. The two terms that are not bounded are

$$\frac{it}{\pi N} \frac{e^{-i\omega_j t}[\tilde{\rho}(\omega_j) - \omega_j]}{\rho(\omega_j)^2 + [\tilde{\rho}(\omega_j) - \omega_j]^2}$$

and

$$\frac{1}{\pi N} F\frac{1}{\pi} \int \frac{e^{-i\omega t} \rho(\omega) d\omega}{(\omega - \omega_j)^2\{\rho(\omega)^2 + [\tilde{\rho}(\omega) - \omega]^2\}}. \tag{47}$$

While it is not entirely obvious that the latter term diverges with t, one can check using the definition of the Hadamard finite part that it behaves as

$$-\frac{t}{\pi N} \frac{e^{-i\omega_j t} \rho(\omega_j)}{\rho(\omega_j)^2 + [\tilde{\rho}(\omega_j) - \omega_j]^2} \tag{48}$$

when $t \to \infty$. Assuming that the denominators of (47) and (48) are of order $\rho(\omega_j)^2$, we indeed find that these terms dominate the other ones responsible for an oscillatory behavior $\sim O(1)$ in Eq. (45) when $t \gg \rho(\omega_j)$.

Plugging this into Eq. (46), we find that the escape probability grows linearly with t in the regime $\rho(\omega) \ll t \ll N\rho(\omega)$ (i.e., $1 \ll tW \ll N$ for a box distribution),

$$\begin{aligned} P_j(t) &\simeq 1 - \left| 1 + \frac{t}{\pi N} \frac{-\rho(\omega_j) + i[\tilde{\rho}(\omega_j) - \omega_j]}{\rho(\omega_j)^2 + [\tilde{\rho}(\omega_j) - \omega_j]^2} \right|^2 \\ &\simeq \Gamma(\omega_j) t, \end{aligned}$$

with the following escape rate (here we reinstate the factors $g\sqrt{\pi}$):

$$\Gamma(\omega) = \frac{2\pi g^2}{N} \frac{\rho(\varepsilon)/(\pi g)^2}{\rho(\varepsilon)^2 + \big[\tilde{\rho}(\varepsilon) - \frac{\varepsilon}{\pi g^2}\big]^2} = 2\pi \left(\frac{g}{\sqrt{N}} \right)^2 \overline{A}(\omega). \tag{49}$$

It is interesting to note that Eq. (49) has a form similar to that given by Fermi's golden rule, with the photon spectral function playing the role of the usual density of states. Moreover, it is the individual coupling strength $g/\sqrt{N}$ and *not* the collective one that enters the escape rate. We now provide an interpretation of that result based on a second-order perturbative approach.

C. Fermi's golden rule for an effective long-range hopping Hamiltonian

To second order, the light-matter coupling term $\hat{V}$ in the TC Hamiltonian (1) affects the bare orbitals as follows. Reinstating the cavity-mode frequency ω_c for clarity, the eigenstates $|j,0\rangle^{(2)}$ read

$$|j,0\rangle^{(2)} = |j,0\rangle + \frac{g}{(\omega_j-\omega_c)\sqrt{N}}|G,1\rangle + \sum_{i\neq j}\frac{g^2}{N(\omega_j-\omega_i)(\omega_j-\omega_c)}|i,0\rangle\,. \tag{50}$$

The photon weight of the perturbed eigenstate $|j,0\rangle^{(2)}$ is $\mathcal{W}(\omega_j) = |\langle G,1|j,0\rangle^{(2)}|^2 = g^2/(\omega_j-\omega_c)^2N$. The perturbative expansion is valid as long as the latter remains small, i.e., when the individual coupling strength $g/\sqrt{N}$ is a small fraction of the detuning between the site j and the cavity. This excludes spin energies too close to the cavity resonance, where a reversible energy exchange between the spin and the cavity would take place (strong-coupling physics). Instead, the perturbative expansion is only relevant for weak couplings. For a box distribution and $g \ll W$, one indeed recovers the perturbative result $\mathcal{W}(\omega_j) = g^2/(\omega_j-\omega_c)^2N$ starting from the exact formula (12). Note that for a spin energy far enough from resonance, i.e., $\omega_j-\omega_c \sim W$, the perturbative criterion $g/(\omega_j-\omega_c)N \ll 1$ is automatically satisfied in the thermodynamic limit.

Starting with an excitation localized on site j at time $t=0$, we would now like to compute the escape probability to other sites i at time t. From energy conservation, one can already expect that these processes imply $\omega_i = \omega_j$, and therefore the perturbative expansion (50) does not appear to be well suited as the third term on the right-hand side diverges. It is instead convenient to use a Schrieffer-Wolff transformation on the Hamiltonian (1), which results in a disentanglement of light and matter degrees of freedom [79]. The new Hamiltonian is written as $\hat{H}' = e^{\hat{S}}\hat{H}e^{-\hat{S}}$. Under the assumption that the eigenvalues of the generator $\hat{S}$ remain small (discussed below), one can expand $\hat{H}'$ in series as $\hat{H}' = \hat{H} + [\hat{S},\hat{H}] + \frac{1}{2}[\hat{S},[\hat{S},\hat{H}]] + \cdots$. Replacing the kinetic energy $\sum_i \omega_i\hat{\sigma}_i^+\hat{\sigma}_i^-$ in Eq. (1) by the equivalent term $\sum_i \omega_i\hat{\sigma}_i^z/2$ for convenience (σ_i^z denotes the third Pauli matrix), the linear coupling $\hat{V}$ can be removed from the expansion with the choice

$$\hat{S} = \sum_j \frac{g}{(\omega_j-\omega_c)\sqrt{N}}(\hat{a}\hat{\sigma}_j^+ - \hat{\sigma}_j^-\hat{a}^\dagger),$$

which provides $[\hat{S},\hat{H}_0] = -\hat{V}$. The new Hamiltonian takes the form

$$\hat{H}' = \hat{H}_0 + \tfrac{1}{2}[\hat{S},\hat{V}] + O(\hat{V}^3), \tag{51}$$

and the condition to be satisfied if one is to keep only the first two terms on the right-hand side of Eq. (51) is therefore $g/\sqrt{N} \ll \omega_j-\omega_c$, which is identical to the condition of validity of the expansion (50). Calculating the commutator $[\hat{S},\hat{V}]$, we obtain

$$\hat{H}' = \sum_i \omega_i\hat{\sigma}_i^+\hat{\sigma}_i^- + \frac{g^2}{2N}\sum_{i,j}\left(\frac{1}{\omega_i-\omega_c}+\frac{1}{\omega_j-\omega_c}\right)\hat{\sigma}_i^+\hat{\sigma}_j^- + \left(\omega_c + \frac{1}{N}\sum_i\frac{g^2}{\omega_i-\omega_c}\hat{\sigma}_i^z\right)\hat{a}^\dagger\hat{a}, \tag{52}$$

up to a constant term. The second term corresponds to an effective hopping between two arbitrarily distant sites, with diverging amplitude when the two sites are in resonance with the cavity. The third term results in a renormalization of the cavity frequency depending on the two-level emitter states. Equivalently, the emitter energies get shifted by cavity photons, which is usually referred to as dispersive Stark shift. This term does not contribute to transitions between states with one excited emitter and zero photon and can therefore be dropped out of the calculation. As eigenstates of $\hat{H}_0$, these states (denoted by $|j\rangle$ for convenience) satisfy $\hat{H}_0|j\rangle = \omega_j|j\rangle$ and $|j(t)\rangle = e^{-i\omega_j t}|j\rangle$. Calling $\hat{V}'$ the second term on the right-hand side of Eq. (52), the Schrödinger equation

$$i\frac{\partial|\Psi(t)\rangle}{\partial t} = \hat{H}'|\Psi(t)\rangle\,,$$

with the ansatz $|\Psi(t)\rangle = \sum_j c_j(t)e^{-i\omega_j t}|j\rangle$, provides the probability amplitudes $c_j(t)$ as solutions of

$$\frac{\partial c_j(t)}{\partial t} = -i\sum_i c_i(t)\langle i|\hat{V}'|j\rangle e^{i(\omega_j-\omega_i)t}. \tag{53}$$

Starting with an excitation on site j at time $t=0$ corresponds to $|\Psi(0)\rangle = |j\rangle$, i.e., $c_j(0)=1$ and $c_{i\neq j}(0)=0$. One can then solve Eq. (53) with this initial condition and sum over all possible final states to obtain the escape probability from site j as

$$P_j(t) = \sum_{i\neq j}|c_i(t)|^2 = 4\sum_{i\neq j}|\langle i|\hat{V}'|j\rangle|^2\frac{\sin^2[(\omega_i-\omega_j)t/2]}{(\omega_i-\omega_j)^2}, \tag{54}$$

which features a sharp peak of width $\sim 1/t$ about $\omega_j=\omega_i$. Under the condition that this characteristic width largely exceeds the mean level spacing $1/\rho(\omega)N$ (equal to W/N for a box distribution), the summation in Eq. (54) can be replaced by an integral. With the density of final states $N\rho(\omega)$ [see Eq. (3)], we obtain

$$P_j(t) = 2tN\int_{\omega_{\min}}^{\omega_{\max}} d\omega\,\rho(\omega)|\langle i|\hat{V}'|j\rangle|^2\xi_j(t,\omega). \tag{55}$$

We also assume that the time t is large enough for the width of the function

$$\xi_j(t,\omega) = \frac{\sin^2[(\omega-\omega_j)t/2]}{(\omega-\omega_j)^2t/2}$$

to be much smaller than the extent of the integration domain $\omega_{\max}-\omega_{\min} \sim 1/\rho(\omega)$ (equal to W for a box distribution), in which case $\xi_j(t,\omega) \to \pi\delta(\omega-\omega_j)$ can be replaced by a δ function. With the matrix element

$$\langle i|\hat{V}'|j\rangle = \frac{g^2}{2N}\left(\frac{1}{\omega_i-\omega_c}+\frac{1}{\omega_j-\omega_c}\right),$$

the escape probability (55) can be written as $P_j(t) = \Gamma(\omega_j)t$, where the escape rate

$$\Gamma(\omega_j) = 2\pi g^2\mathcal{W}(\omega_j)\rho(\omega_j) = 2\pi(g/\sqrt{N})^2A(\omega_j)$$

has the same form as in Eq. (49). Note that the probability $P_j(t)$ must remain small compared to one, and the conditions $1 \ll tW \ll N$ (for a box distribution) and $P_j(t) \ll 1$ ensuring validity of Fermi's golden rule can be satisfied simultaneously

in the thermodynamic limit, provided the coupling is weak enough ($g \ll W$).

D. Physical properties of the escape dynamics

The g dependence of the escape rate $\Gamma(\omega_j)$ given by Eq. (49) exhibits some interesting features, which we now illustrate using our usual box distribution of width W. In this case, we recall that $\rho = 1/W$ for $\omega_j \in [-W/2, W/2]$ and $\rho = 0$ otherwise, and the Hilbert transform $\tilde{\rho}$ is given in Eq. (29). Injecting the excitation in the middle of that distribution, i.e., $\omega_j = 0$, the escape rate is independent of g and reads $\Gamma(0) = \frac{2W}{\pi N}$, which can be made *arbitrary large* by increasing the disorder strength W. Conversely, injecting exactly on the edges of the distribution $\omega_j = \pm W/2$, the escape rate vanishes for all values of g, i.e., $\Gamma(\pm W/2) = 0$. In all other cases, the escape rate grows as $\sim 2\pi g^4/\omega_j^2 W$ for weak couplings $g \ll W$, reaches a maximum $2W/\pi N$ for

$$g = \sqrt{\frac{\omega_j}{\pi \tilde{\rho}(\omega_j)}}$$

(which typically corresponds to intermediate coupling strengths $g \sim W$), and then saturates to a lower, g-independent value

$$\frac{2W}{\pi N}\left(\frac{1}{1 + W^2\tilde{\rho}^2(\omega_j)}\right)$$

for strong couplings $g \gg W$. It is remarkable here that both the maximum escape rate and the saturation value increase with the disorder strength W, which originates from the enhancement of the photon weight of the dark states [or equivalently the contribution of the dark states to the spectral function $A(\omega)$], as can be seen from Eqs. (12) and (15).

The disorder-averaged escape rate

$$\begin{aligned}\mathbb{E}[\Gamma(\omega_j)] = &= \frac{1}{W}\int_{-W/2}^{W/2} \Gamma(\omega) d\omega \\ &= \frac{2\pi g^2}{NW}(1 - \mathcal{W}_+ - \mathcal{W}_-) \end{aligned} \tag{56}$$

exhibits similar features and is shown in Fig. 5(a). Note that since the photon weight is a normalized quantity, i.e., $\sum_{a=1}^{N+1} \mathcal{W}_a = 1$, the quantity in parentheses entering the right-hand side of Eq. (56) is nothing but the photon weight of the dark states [see Eq. (44)] integrated over the support of ρ. For weak couplings one finds $\mathbb{E}[\Gamma] \sim \frac{2\pi g^2}{NW}$ (grows as $\sim g^2$) and $\mathbb{E}[\Gamma]$ reaches a maximum at intermediate coupling strengths $g \sim W$ and then saturates for strong couplings to a lower, g-independent value $\frac{\pi W}{6N}$, which increases with W.

VII. OUT-OF-EQUILIBRIUM TRANSPORT

Now that we have identified and discussed cavity-protection effects for the escape probability, it is interesting to look at the excitation current flowing through the system of emitters in an out-of-equilibrium situation. Such a situation occurs when connecting two particular emitter sites to Markovian baths: The source injects excitations at site $j = 1$, while the drain extracts excitations at site $j = N$. (In this section we do not assume that the bare energies are sorted in increasing order, so the energies of the in and out sites ω_1 and ω_N need not be the minimum and maximum bare energies.) Since we are working in the single-excitation subspace, we can replace the spin operators by fermionic ones for simplicity, i.e., $\hat{\sigma}_i^- \to \hat{\sigma}_i$ and $\hat{\sigma}_i^+ \to \hat{\sigma}_i^\dagger$ ($i = 1, \ldots, N$), with $\{\hat{\sigma}_i, \hat{\sigma}_j^\dagger\} = \delta_{i,j}$. The excitation current and populations across the system of emitters are computed using the nonequilibrium Green's function formalism. The system is described by the Hamiltonian $\hat{H}_{\text{neq}} = \hat{H} + \hat{H}_{\text{r}}$, with $\hat{H}$ given by Eq. (1) and

$$\begin{aligned}\hat{H}_r = &\sum_\alpha \omega_\alpha \hat{\sigma}_{\alpha,\text{in}}^\dagger \hat{\sigma}_{\alpha,\text{in}} + \sum_\alpha \omega_\alpha \hat{\sigma}_{\alpha,\text{out}}^\dagger \hat{\sigma}_{\alpha,\text{out}} \\ &+ \sum_\alpha \lambda_\alpha^{\text{in}}(\hat{\sigma}_1 \hat{\sigma}_{\alpha,\text{in}}^\dagger + \hat{\sigma}_{\alpha,\text{in}}\hat{\sigma}_1^\dagger) \\ &+ \sum_\alpha \lambda_\alpha^{\text{out}}(\hat{\sigma}_N \hat{\sigma}_{\alpha,\text{out}}^\dagger + \hat{\sigma}_{\alpha,\text{out}}\hat{\sigma}_N^\dagger).\end{aligned}$$

Here α denotes some quantum number running over a continuum of states in each reservoir. For a given function f_α, summations of the type $\sum_\alpha f_\alpha$ are replaced with $\int d\omega\, d(\omega) f(\omega)$, with $d(\omega)$ the density of states in the reservoirs and $\omega \equiv \omega_\alpha$ the energy of the state α. The operator $\hat{\sigma}_{\alpha,l}$ ($\hat{\sigma}_{\alpha,l}^\dagger$) annihilates (creates) a fermion in the reservoir $l = \text{in, out}$ and the real parameters $\lambda_\alpha^{\text{in}}$ and $\lambda_\alpha^{\text{out}}$ are the coupling strengths between the reservoirs and the two ends of the system. The steady-state excitation current flowing through the emitters can be computed from either the input current

$$J_{\text{in}} = \left\langle \frac{\partial \hat{N}_{\text{in}}}{\partial t} \right\rangle = i\langle [\hat{H}_{\text{neq}}, \hat{N}_{\text{in}}] \rangle$$

or the output current

$$J_{\text{out}} = \left\langle \frac{\partial \hat{N}_{\text{out}}}{\partial t} \right\rangle = i\langle [\hat{H}_{\text{neq}}, \hat{N}_{\text{out}}] \rangle,$$

since these two are equal in magnitude. Here $\hat{N}_l = \sum_\alpha \hat{\sigma}_{\alpha,l}^\dagger \hat{\sigma}_{\alpha,l}$ is the number of fermions in the reservoir $l = \text{in, out}$ and $\langle \cdots \rangle$ is the expectation value in the steady state [80].

We force injection and extraction of particles at the first and last sites, respectively, assuming $n_{\text{in}}(\omega) \equiv \langle \hat{\sigma}_{\alpha,\text{in}}^\dagger \hat{\sigma}_{\alpha,\text{in}} \rangle = 1$ and $n_{\text{out}}(\omega) \equiv \langle \hat{\sigma}_{\alpha,\text{out}}^\dagger \hat{\sigma}_{\alpha,\text{out}} \rangle = 0$ for all energies ω in the range of interest. Following Ref. [81], it can be shown that, in this case, the input and output currents take the forms $J_{\text{in}} = -\Gamma_{\text{in}}(1 - n_1)$ and $J_{\text{out}} = \Gamma_{\text{out}} n_N$, with $J_{\text{in}} = -J_{\text{out}}$, $\Gamma_{\text{in}} \equiv 2\pi d(\omega)\lambda_{\text{in}}^2(\omega)$ and $\Gamma_{\text{out}} \equiv 2\pi d(\omega)\lambda_{\text{out}}^2(\omega)$ the injection and extraction rates assumed to be frequency independent (Markovian baths), and

$$n_j = \int \frac{d\omega}{2\pi} \text{Im}[G_{j,j}^<(\omega)] \tag{57}$$

the population on site j [82]. Here $G_{i,j}^<(\omega)$ denotes the lesser Green's function, which is defined in the Appendix.

A. Equations of motion

The transport properties of the model are thus encoded in the nonequilibrium Green's function $G_{i,j}^<(\omega)$. The latter can be computed by first deriving the equations of motion of the retarded and advanced Green's functions, which are themselves obtained by computing their first time derivative

(and therefore the commutator of $\hat{\sigma}_i$ with the different parts of the Hamiltonian $\hat{H}_{\rm neq}$ [81]). In the frequency domain, the equations of motion can be written in the Dyson form [80]

$$\sum_k \left\{\left[G^{0\beta}_{i,k}(\omega)\right]^{-1} - \Sigma^{\beta}_{i,k}(\omega)\right\} G^{\beta}_{k,j}(\omega) = \delta_{i,j}, \tag{58}$$

with $\beta = \mathrm{A}, \mathrm{R}$, the noninteracting Green's functions $G^{0\beta}_{i,j}(\omega)$ given in the Appendix, and the self-energies

$$\Sigma^{\mathrm{R}}_{j,k}(\omega) = \frac{g^2}{N} D^{\mathrm{R}}_0(\omega) - \frac{i}{2}\delta_{j,k}(\delta_{j,1}\Gamma_{\rm in} + \delta_{j,N}\Gamma_{\rm out})$$

and $\Sigma^{\mathrm{A}}_{j,k}(\omega) = [\Sigma^{\mathrm{R}}_{j,k}(\omega)]^*$. Here D^{R}_0 denotes the retarded noninteracting cavity Green's function also given in the Appendix. The lesser Green's function is obtained from the Keldysh equation

$$G^{<}_{i,j}(\omega) = \sum_{k,p} G^{\mathrm{R}}_{i,k}(\omega)\Sigma^{<}_{k,p}(\omega)G^{\mathrm{A}}_{p,j}(\omega),$$

with the lesser self-energy

$$\Sigma^{<}_{k,p}(\omega) = i\Gamma_{\rm in}\delta_{k,p}\delta_{k,1}. \tag{59}$$

Another useful quantity is the cavity photon population given by [82]

$$n_c = \int \frac{d\omega}{2\pi} \mathrm{Im}[D^{<}(\omega)].$$

In order to compute the lesser cavity photon Green's function $D^{<}(\omega)$, we proceed as before and derive the equations of motion of the retarded and advanced cavity Green's functions. In the frequency domain, these equations of motion take the form

$$\left\{\left[D^{\beta}_0(\omega)\right]^{-1} - \Pi^{\beta}(\omega)\right\} D^{\beta}(\omega) = 1,$$

with $\beta = \mathrm{A}, \mathrm{R}$, and the cavity self-energies

$$\Pi^{\mathrm{R}}(\omega) = \frac{g^2}{N}\sum_j \frac{1}{\omega - \omega_j + \frac{i}{2}(\delta_{j,1}\Gamma_{\rm in} + \delta_{j,N}\Gamma_{\rm out})}$$

and $\Pi^{\mathrm{A}}(\omega) = [\Pi^{\mathrm{R}}(\omega)]^*$. Again, the lesser cavity Green's function is obtained from the Keldysh equation $D^{<}(\omega) = D^{\mathrm{R}}(\omega)\Pi^{<}(\omega)D^{\mathrm{A}}(\omega)$, with

$$\Pi^{<}(\omega) = \frac{g^2}{N}\frac{i\Gamma_{\rm in}}{(\omega-\omega_1)^2 + (\Gamma_{\rm in}/2)^2}.$$

B. Analytical formulas for the current and populations

The Dyson equation (58) can be solved exactly using matrix inversion carried out with the Sherman-Morrison formula. This leads to

$$G^{\mathrm{R}}_{i,j}(\omega) = \frac{g^2}{N}\frac{D^{\mathrm{R}}(\omega)}{(\omega-\tilde{\omega}_i)(\omega-\tilde{\omega}_j)} \quad \text{for } i \neq j,$$

$$G^{\mathrm{R}}_{i,i}(\omega) = \frac{1}{\omega-\tilde{\omega}_i} + \frac{g^2}{N}\frac{D^{\mathrm{R}}(\omega)}{(\omega-\tilde{\omega}_i)^2}, \tag{60}$$

and $G^{\mathrm{A}}_{i,j}(\omega) = [G^{\mathrm{R}}_{i,j}(\omega)]^*$, with $\tilde{\omega}_1 = \omega_1 - \frac{i\Gamma_{\rm in}}{2}$, $\tilde{\omega}_N = \omega_N - \frac{i\Gamma_{\rm out}}{2}$, and $\tilde{\omega}_j = \omega_j$ for all $j \neq 1, N$. In order to compute the steady-state populations and current according to Eq. (57), we use the Keldysh equation $\underline{G}^{<}(\omega) = \underline{G}^{\mathrm{R}}(\omega)\underline{\Sigma}^{<}(\omega)\underline{G}^{\mathrm{A}}(\omega)$, with $\underline{\Sigma}^{<}(\omega)$ given by Eq. (59) and $\underline{G}^{\mathrm{R}}(\omega)$ given by Eq. (60). The integration in frequency domain is performed using the residue theorem, with the factorization of the cavity-mode Green's functions,

$$D^{\mathrm{R}}(z) = \frac{\prod_{j=1}^{N}(z-\tilde{\omega}_j)}{\prod_{a=1}^{N+1}(z-\epsilon_a)}, \quad D^{\mathrm{A}}(z) = [D^{\mathrm{R}}(z)]^*,$$

and ϵ_a the $N+1$ solutions of the polynomial equation

$$z\prod_{j=1}^{N}(z-\tilde{\omega}_j) - \frac{g^2}{N}\sum_{j=1}^{N}\prod_{i\neq j}(z-\tilde{\omega}_j) = 0.$$

These solutions all have negative imaginary parts and correspond to the eigenvalues of the complex symmetric (non-Hermitian) arrowhead matrix

$$\left(\begin{array}{ccccc|c} \tilde{\omega}_1 & 0 & \cdots & 0 & 0 & g/\sqrt{N} \\ 0 & \tilde{\omega}_2 & \ddots & 0 & 0 & g/\sqrt{N} \\ \vdots & \ddots & \ddots & \ddots & \vdots & \vdots \\ 0 & 0 & \ddots & \tilde{\omega}_{N-1} & 0 & g/\sqrt{N} \\ 0 & 0 & \cdots & 0 & \tilde{\omega}_N & g/\sqrt{N} \\ \hline g/\sqrt{N} & g/\sqrt{N} & \cdots & g/\sqrt{N} & g/\sqrt{N} & 0 \end{array}\right). \tag{61}$$

The real part of these eigenvalues exhibits a structure similar to the equilibrium case (without coupling to the reservoirs): $N-1$ dark states with energies comprised between $-W/2$ and $W/2$, and two polaritons emerging from the continuum of dark states for $g \gtrsim W/2$. In contrast to the equilibrium case, these eigenstates exhibit a finite imaginary part (lifetime) due to the coupling to the two reservoirs. Using the results of Secs. VII A and VII B, the integration in Eq. (57) provides the population at site $j \neq 1$,

$$n_j = \Gamma_{\rm in}\frac{g^4}{N^2}\sum_a \frac{\tau_a\phi_a}{(\epsilon_a-\tilde{\omega}_j)(\epsilon_a-\tilde{\omega}_j^*)}, \tag{62}$$

the population at the injection site $j = 1$,

$$\begin{aligned} n_1 = 1 &+ \Gamma_{\rm in}\frac{g^4}{N^2}\sum_a \frac{\tau_a\phi_a}{(\epsilon_a-\tilde{\omega}_1)(\epsilon_a-\tilde{\omega}_1^*)} \\ &+ \frac{g^4}{N^2}\frac{\prod_{k\neq 1}(\tilde{\omega}_1-\tilde{\omega}_k)(\tilde{\omega}_1-\tilde{\omega}_k^*)}{\prod_a(\epsilon_a-\tilde{\omega}_1)(\epsilon_a^*-\tilde{\omega}_1)} \\ &+ \frac{2g^2}{N}\mathrm{Re}\left\{\frac{\prod_{k\neq 1}(\tilde{\omega}_1-\tilde{\omega}_k^*)}{\prod_a(\tilde{\omega}_1-\epsilon_a^*)}\right\}, \end{aligned}$$

and the population of the cavity mode,

$$n_c = \Gamma_{\rm in}\frac{g^2}{N}\sum_a \tau_a\phi_a,$$

with $\tau_a \equiv -1/2\,\mathrm{Im}(\epsilon_a)$ the lifetime of the eigenstates and

$$\phi_a = \frac{\prod_{k\neq 1}(\epsilon_a-\tilde{\omega}_k)(\epsilon_a-\tilde{\omega}_k^*)}{\prod_{a'\neq a}(\epsilon_a-\epsilon_{a'})(\epsilon_a-\epsilon_{a'}^*)}.$$

Importantly, we find that the total population $\mathcal{N} = n_c + \sum_{j=1}^{N} n_j = O(N)$, which violates the single-excitation assumption. Our fermion model for transport thus does not map onto the disordered TC model. A proper rescaling of the

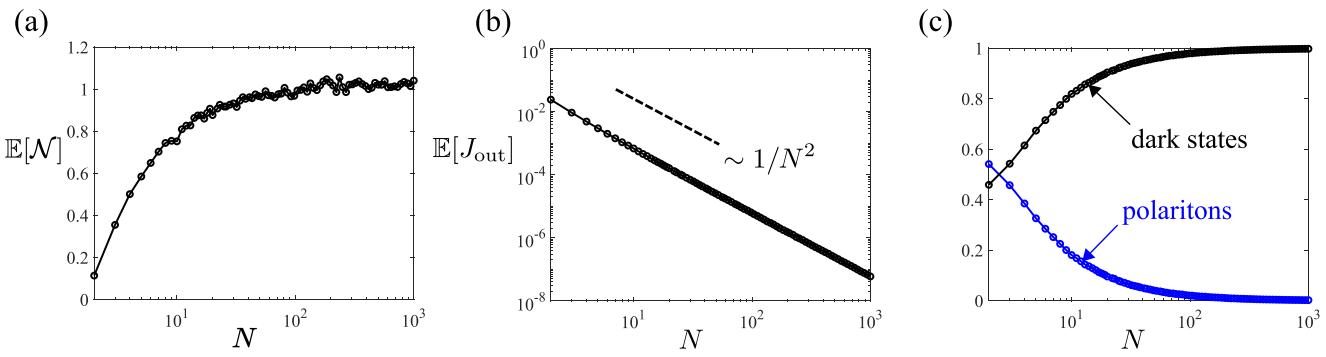

FIG. 13. Out-of-equilibrium transport: (a) disorder-averaged (over 2000 configurations) total population $\mathbb{E}[\mathcal{N}]$, (b) output current $\mathbb{E}[J_{\rm out}]$, and (c) proportion of the current carried by the different eigenstates, as a function of N for $g = 1$. The other parameters are $\Gamma_{\rm in} = 0.1/N^2$ and $\Gamma_{\rm out} = 1$.

current injection rate $\Gamma_{\rm in} \to \tilde{\Gamma}_{\rm in}/N^2$ (while keeping $\tilde{\Gamma}_{\rm in}$ fixed) allows us to circumvent this issue as it results in a total population $O(1)$ [Fig. 13(a)]. This ensures that the system remains in the single-excitation subspace so that the identification of our simple fermionic model for transport with the disorder TC model holds.

C. Cavity-protected transport

Using this rescaling of the injection rate and averaging the steady-state output current

$$J_{\rm out} = \Gamma_{\rm out} n_N = \Gamma_{\rm out} \tilde{\Gamma}_{\rm in} \frac{g^4}{N^4} \sum_a \frac{\tau_a \phi_a}{(\epsilon_a - \tilde{\omega}_N)(\epsilon_a - \tilde{\omega}_N^*)} \quad (63)$$

over disorder, we find that $\mathbb{E}[J_{\rm out}] \sim 1/N^2$ [Fig. 13(b)]. This can be understood from Eq. (63) by observing numerically that the lifetime of the eigenstates $\tau_a \sim N^2$. Moreover, since Eq. (63) involves a summation over the eigenstates of the matrix (61), one can easily extract the contribution of these eigenstates to the disorder-averaged current. While for small N the latter is equally carried by polaritons and dark states, we find that it is fully dominated by the dark states in the thermodynamic limit [Fig. 13(c)]. For a single disorder realization, fixed N, and weak coupling $g \ll W$, the current scales as $\sim g^4$, as can be seen from Eq. (63). Interestingly, after disorder averaging we find that $\mathbb{E}[J_{\rm out}] \sim g^2$, similarly to the escape rate discussed in Sec. VI D. Output current and escape rate share common features also beyond weak couplings [see Figs. 5(a) and 5(b)]: $\mathbb{E}[J_{\rm out}]$ reaches a maximum for intermediate coupling strengths $g \sim W$ and then saturates to a slightly lower value for strong couplings. Importantly, the value of the plateau is found to increase with W, which means that not only does the out-of-equilibrium current exhibit some robustness against disorder, but also that the latter can be used to enhance transport for large couplings $g \gtrsim W$.

VIII. CONCLUSION

We have investigated in detail a class of large arrowhead matrices that are relevant to many physical systems, ranging from molecular junctions to central-spin problems and cavity QED. We have derived asymptotically exact formulas in the thermodynamic limit for different quantities of physical interest such as the spectrum, average energy shifts, inverse participation ratio, and correlation functions. We have shown that the spectrum and the distribution of energy spacing exhibit characteristics usually associated with the critical point of disordered hopping models for Anderson localization-delocalization transitions. We have studied how those peculiar spectral properties are connected to dynamical quantities such as the escape probability and the out-of-equilibrium current, showing that the latter can be efficiently protected by the cavity. Even more significantly, it was shown that disorder can help transport for strong enough couplings. Interesting perspectives include experimentally relevant unbounded disorder distributions (e.g., Gaussian), the effect of dissipation that would typically be included by adding finite imaginary parts to the diagonal elements of the arrowhead matrix Hamiltonian, and many-body effects occurring for larger excitation densities. It is another exciting prospect to investigate whether the combined effects of disorder, light-matter coupling, and particle statistics could lead to nonclassical states of light when driving the cavity with a laser field or upon injecting and removing spin excitations in a transport situation.

ACKNOWLEDGMENTS

We are grateful to Fausto Borgonovi, Giuseppe Luca Celardo, Thibault Chervy, Alexandre Faribault, Francesco Mattiotti, Puneet Murthy, and Deepankur Thureja for stimulating discussions and to Andrea Maroncelli for joint work on closely related projects and comments on the manuscript. This work was supported by the ANR "ERA-NET QuantERA" Project "RouTe" (Project No. ANR-18-QUAN-0005-01). G.P. acknowledges support from the Institut Universitaire de France. Research was carried out using computational resources of the Centre de Calcul de l'Université de Strasbourg.

APPENDIX

In this Appendix we provide definitions of the different Green's functions used throughout the paper, as well as a detailed derivation of the mean energy shift given by Eq. (25b).

The different Green's functions are defined through the evolution operator $\hat{G}(t) = e^{-i\hat{H}t}$, which is an $(N+1)\times(N+1)$

unitary matrix, i.e., $\hat{G}^\dagger(t) = \hat{G}^{-1}(t) = \hat{G}(-t)$. They correspond to the components of that matrix

$$G_{i,j}(t) = \langle i,0|\hat{G}(t)|j,0\rangle = \langle \hat{\sigma}_i^-(t)\hat{\sigma}_j^+(0)\rangle \tag{A1a}$$

for $1 \leqslant i, j \leqslant N$,

$$G_{j,N+1}(t) = \langle j,0|\hat{G}(t)|G,1\rangle = \langle \hat{\sigma}_j^-(t)\hat{a}^\dagger(0)\rangle \tag{A1b}$$

for $1 \leqslant j \leqslant N$, and

$$D(t) \equiv G_{N+1,N+1}(t) = \langle G,1|\hat{G}(t)|G,1\rangle = \langle \hat{a}(t)\hat{a}^\dagger(0)\rangle, \tag{A1c}$$

where $\langle\cdots\rangle = \langle\cdots\rangle G,0$ denotes the expectation value in the ground state $|G,0\rangle$ of both Hamiltonians $\hat{H}_0$ and $\hat{H}$. The operators $\hat{\sigma}_j^\pm(t) = e^{i\hat{H}t}\hat{\sigma}_j^\pm e^{-i\hat{H}t}$ and $\hat{a}^{(\dagger)}(t) = e^{i\hat{H}t}\hat{a}^{(\dagger)}e^{-i\hat{H}t}$ are defined in the Heisenberg picture. In order to simplify notation, we call $D(t)$ the cavity photon Green's function throughout the paper, which corresponds to the $(N+1)$th element of the evolution operator. We introduce the Fourier transform $\hat{G}(\omega) = \int dt\, e^{i\omega t}\hat{G}(t)$, where $\hat{G}(t) = i[\hat{G}^{\mathrm{R}}(t) - \hat{G}^{\mathrm{A}}(t)]$ can be expressed as the sum of a retarded $\hat{G}^{\mathrm{R}}(t) = -i\theta(t)e^{-i\hat{H}t}$ and an advanced $\hat{G}^{\mathrm{A}}(t) = i\theta(-t)e^{-i\hat{H}t}$ propagator (θ denotes the Heaviside function) in such a way that

$$\hat{G}^{\mathrm{R}}(\omega) = \frac{1}{\omega - \hat{H} + i0^+},$$
$$\hat{G}^{\mathrm{A}}(\omega) = \frac{1}{\omega - \hat{H} + i0^-}.$$

Of particular interest is the photon spectral function

$$A(\omega) \equiv -\frac{1}{\pi}\mathrm{Im}D^{\mathrm{R}}(\omega),$$

which is a positive-definite operator characterizing the spectrum of the system and which can be directly accessed in experiments by measuring the cavity transmission or fluorescence emission spectra. It is also often convenient to introduce the lesser and greater Green's functions as

$$G_{i,j}^<(t) = i\langle\hat{\sigma}_j^+(0)\hat{\sigma}_i^-(t)\rangle,$$
$$G_{i,j}^>(t) = -i\langle\hat{\sigma}_i^-(t)\hat{\sigma}_j^+(0)\rangle.$$

Note that $G_{i,j}^>(t)$ corresponds up to a $-i$ factor to $G_{i,j}(t)$ as defined in Eq. (A1a) at equilibrium (in the absence of coupling to external reservoirs as in Sec. VII). In this situation, $G_{i,j}^<(t)$ vanishes since $\langle\cdots\rangle$ denotes the expectation value in the ground state $|G,0\rangle$. Similar definitions hold for the cavity photon Green's functions:

$$D^<(t) = i\langle\hat{a}^\dagger(0)\hat{a}(t)\rangle,$$
$$D^>(t) = -i\langle\hat{a}(t)\hat{a}^\dagger(0)\rangle.$$

Note that retarded and advanced functions are related to lesser and greater ones by

$$\hat{G}^{\mathrm{R}}(t) = \theta(t)[\hat{G}^>(t) - \hat{G}^<(t)],$$
$$\hat{G}^{\mathrm{A}}(t) = \theta(-t)[\hat{G}^<(t) - \hat{G}^>(t)],$$

and similarly for cavity photons. The noninteracting retarded and advanced Green's functions, i.e., in the absence of light-matter interactions and coupling to external reservoirs, read

$$G_{i,j}^{0\mathrm{R}}(\omega) = \frac{\delta_{i,j}}{\omega - \omega_i + i0^+},$$
$$G_{i,j}^{0\mathrm{A}}(\omega) = \left[G_{i,j}^{0\mathrm{R}}(\omega)\right]^*$$

for spins and

$$D_0^{\mathrm{R}}(\omega) = \frac{1}{\omega + i0^+},$$
$$D_0^{\mathrm{A}}(\omega) = \left[D_0^{\mathrm{R}}(\omega)\right]^*$$

for cavity photons (when treated as fermions as in Sec. VII).

[1] M. L. Mehta, *Random Matrices* (Elsevier, Amsterdam, 2004).

[2] G. W. Anderson, A. Guionnet, and O. Zeitouni, *An Introduction to Random Matrices* (Cambridge University Press, Cambridge, 2010), Vol. 118.

[3] P. J. Forrester, *Log-Gases and Random Matrices (LMS-34)* (Princeton University Press, Princeton, 2010).

[4] G. Akemann, J. Baik, and P. Di Francesco, *The Oxford Handbook of Random Matrix Theory* (Oxford University Press, Oxford, 2011).

[5] T. Tao, *Topics in Random Matrix Theory* (American Mathematical Society, Providence, 2012), Vol. 132.

[6] D. P O'Leary and G. Stewart, Computing the eigenvalues and eigenvectors of symmetric arrowhead matrices, J. Comput. Phys. **90**, 497 (1990).

[7] G. A. Gravvanis, An approximate inverse matrix technique for arrowhead matrices, Int. J. Comput. Math. **70**, 35 (1998).

[8] H. S. Najafi, S. Edalatpanah, and G. A. Gravvanis, An efficient method for computing the inverse of arrowhead matrices, Appl. Math. Lett. **33**, 1 (2014).

[9] N. J. Stor, I. Slapničar, and J. L. Barlow, Accurate eigenvalue decomposition of real symmetric arrowhead matrices and applications, Linear Algebra Appl. **464**, 62 (2015).

[10] S. E. Sussman-Fort, The reconstruction of bordered-diagonal and Jacobi matrices from spectral data, J. Franklin Inst. **314**, 271 (1982).

[11] H. Pickmann, J. Egana, and R. L. Soto, Extremal inverse eigenvalue problem for bordered diagonal matrices, Linear Algebra Appl. **427**, 256 (2007).

[12] R. J. Elliott, J. A. Krumhansl, and P. L. Leath, The theory and properties of randomly disordered crystals and related physical systems, Rev. Mod. Phys. **46**, 465 (1974).

[13] J. W. Gadzuk, Localized vibrational modes in Fermi liquids. general theory, Phys. Rev. B **24**, 1651 (1981).

[14] Y. Vinkler-Aviv, A. Schiller, and N. Andrei, Single-molecule-mediated heat current between an electronic and a bosonic bath, Phys. Rev. B **89**, 024307 (2014).
[15] S. Y. Quek, M. Kamenetska, M. L. Steigerwald, H. J. Choi, S. G. Louie, M. S. Hybertsen, J. B. Neaton, and L. Venkataraman, Mechanically controlled binary conductance switching of a single-molecule junction, Nat. Nanotechnol. **4**, 230 (2009).
[16] M. A. Reed, C. Zhou, C. J. Muller, T. P. Burgin, and J. M. Tour, Conductance of a molecular junction, Science **278**, 252 (1997).
[17] N. J. Tao, Electron transport in molecular junctions, Nat. Nanotechnol. **1**, 173 (2006).
[18] G. C. Solomon, C. Herrmann, T. Hansen, V. Mujica, and M. A. Ratner, Exploring local currents in molecular junctions, Nat. Chem. **2**, 223 (2010).
[19] M. Galperin, A. Nitzan, and M. A. Ratner, Heat conduction in molecular transport junctions, Phys. Rev. B **75**, 155312 (2007).
[20] L. Cui, S. Hur, Z. A. Akbar, J. C. Klöckner, W. Jeong, F. Pauly, S.-Y. Jang, P. Reddy, and E. Meyhofer, Thermal conductance of single-molecule junctions, Nature (London) **572**, 628 (2019).
[21] S. V. Aradhya and L. Venkataraman, Single-molecule junctions beyond electronic transport, Nat. Nanotechnol. **8**, 399 (2013).
[22] W. Zhu, R. Esteban, A. G. Borisov, J. J. Baumberg, P. Nordlander, H. J. Lezec, J. Aizpurua, and K. B. Crozier, Quantum mechanical effects in plasmonic structures with sub-nanometre gaps, Nat. Commun. **7**, 11495 (2016).
[23] B. J. van Wees, H. van Houten, C. W. J. Beenakker, J. G. Williamson, L. P. Kouwenhoven, D. van der Marel, and C. T. Foxon, Quantized Conductance of Point Contacts in a Two-Dimensional Electron Gas, Phys. Rev. Lett. **60**, 848 (1988).
[24] D. A. Wharam, T. J. Thornton, R. Newbury, M. Pepper, H. Ahmed, J. E. F. Frost, D. G. Hasko, D. C. Peacock, D. A. Ritchie, and G. A. C. Jones, One-dimensional transport and the quantisation of the ballistic resistance, J. Phys. C **21**, L209 (1988).
[25] F. Benz, M. K. Schmidt, A. Dreismann, R. Chikkaraddy, Y. Zhang, A. Demetriadou, C. Carnegie, H. Ohadi, B. de Nijs, R. Esteban, J. Aizpurua, and J. J. Baumberg, Single-molecule optomechanics in "picocavities", Science **354**, 726 (2016).
[26] M. Gaudin, Diagonalisation d'une classe d'Hamiltoniens de spin, J. Phys. (Paris) **37**, 1087 (1976).
[27] N. V. Prokof'ev and P. C. E. Stamp, Theory of the spin bath, Rep. Prog. Phys. **63**, 669 (2000).
[28] H.-P. Breuer, D. Burgarth, and F. Petruccione, Non-Markovian dynamics in a spin star system: Exact solution and approximation techniques, Phys. Rev. B **70**, 045323 (2004).
[29] A. Khaetskii, D. Loss, and L. Glazman, Electron spin evolution induced by interaction with nuclei in a quantum dot, Phys. Rev. B **67**, 195329 (2003).
[30] W. A. Coish and D. Loss, Hyperfine interaction in a quantum dot: Non-Markovian electron spin dynamics, Phys. Rev. B **70**, 195340 (2004).
[31] A. A. Zhukov, S. V. Remizov, W. V. Pogosov, and Y. E. Lozovik, Algorithmic simulation of far-from-equilibrium dynamics using quantum computer, Quantum Inf. Process. **17**, 223 (2018).
[32] R. Hanson, V. V. Dobrovitski, A. E. Feiguin, O. Gywat, and D. D. Awschalom, Coherent dynamics of a single spin interacting with an adjustable spin bath, Science **320**, 352 (2008).
[33] Y. Kaluzny, P. Goy, M. Gross, J. M. Raimond, and S. Haroche, Observation of Self-Induced Rabi Oscillations in Two-Level Atoms Excited Inside a Resonant Cavity: The Ringing Regime of Superradiance, Phys. Rev. Lett. **51**, 1175 (1983).
[34] M. G. Raizen, R. J. Thompson, R. J. Brecha, H. J. Kimble, and H. J. Carmichael, Normal-Mode Splitting and Linewidth Averaging for Two-State Atoms in an Optical Cavity, Phys. Rev. Lett. **63**, 240 (1989).
[35] P. Törmä and W. L. Barnes, Strong coupling between surface plasmon polaritons and emitters: A review, Rep. Prog. Phys. **78**, 013901 (2014).
[36] M. Tavis and F. W. Cummings, Exact solution for an *N*-molecule–radiation-field Hamiltonian, Phys. Rev. **170**, 379 (1968).
[37] J. M. Fink, R. Bianchetti, M. Baur, M. Göppl, L. Steffen, S. Filipp, P. J. Leek, A. Blais, and A. Wallraff, Dressed Collective Qubit States and the Tavis-Cummings Model in Circuit QED, Phys. Rev. Lett. **103**, 083601 (2009).
[38] D. Shapiro, P. Macha, A. Rubtsov, and A. Ustinov, Dispersive response of a disordered superconducting quantum metamaterial, Photonics **2**, 449 (2015).
[39] Y. Kubo, F. R. Ong, P. Bertet, D. Vion, V. Jacques, D. Zheng, A. Dréau, J.-F. Roch, A. Auffeves, F. Jelezko, J. Wrachtrup, M. F. Barthe, P. Bergonzo, and D. Esteve, Strong Coupling of a Spin Ensemble to a Superconducting Resonator, Phys. Rev. Lett. **105**, 140502 (2010).
[40] T. Astner, S. Nevlacsil, N. Peterschofsky, A. Angerer, S. Rotter, S. Putz, J. Schmiedmayer, and J. Majer, Coherent Coupling of Remote Spin Ensembles via a Cavity Bus, Phys. Rev. Lett. **118**, 140502 (2017).
[41] G. S. Agarwal, Vacuum-Field Rabi Splittings in Microwave Absorption by Rydberg Atoms in a Cavity, Phys. Rev. Lett. **53**, 1732 (1984).
[42] Y. Zhu, D. J. Gauthier, S. E. Morin, Q. Wu, H. J. Carmichael, and T. W. Mossberg, Vacuum Rabi Splitting as a Feature of Linear-Dispersion Theory: Analysis and Experimental Observations, Phys. Rev. Lett. **64**, 2499 (1990).
[43] F. Dimer, B. Estienne, A. S. Parkins, and H. J. Carmichael, Proposed realization of the Dicke-model quantum phase transition in an optical cavity QED system, Phys. Rev. A **75**, 013804 (2007).
[44] Z. Zhiqiang, C. H. Lee, R. Kumar, K. J. Arnold, S. J. Masson, A. S. Parkins, and M. D. Barrett, Nonequilibrium phase transition in a spin-1 Dicke model, Optica **4**, 424 (2017).
[45] Z. Zhang, C. H. Lee, R. Kumar, K. J. Arnold, S. J. Masson, A. L. Grimsmo, A. S. Parkins, and M. D. Barrett, Dicke-model simulation via cavity-assisted Raman transitions, Phys. Rev. A **97**, 043858 (2018).
[46] R. Houdré, R. P. Stanley, and M. Ilegems, Vacuum-field Rabi splitting in the presence of inhomogeneous broadening: Resolution of a homogeneous linewidth in an inhomogeneously broadened system, Phys. Rev. A **53**, 2711 (1996).
[47] F. M. Marchetti, J. Keeling, M. H. Szymańska, and P. B. Littlewood, Thermodynamics and Excitations of Condensed Polaritons in Disordered Microcavities, Phys. Rev. Lett. **96**, 066405 (2006).
[48] F. M. Marchetti, J. Keeling, M. H. Szymańska, and P. B. Littlewood, Absorption, photoluminescence, and resonant Rayleigh scattering probes of condensed microcavity polaritons, Phys. Rev. B **76**, 115326 (2007).

[49] Z. Kurucz, J. H. Wesenberg, and K. Mølmer, Spectroscopic properties of inhomogeneously broadened spin ensembles in a cavity, Phys. Rev. A **83**, 053852 (2011).

[50] P. Kirton, M. M. Roses, J. Keeling, and E. G. D. Torre, Introduction to the Dicke model: From equilibrium to nonequilibrium, and vice versa, Adv. Quantum Technol. **2**, 1800043 (2019).

[51] V. V. Temnov and U. Woggon, Superradiance and Subradiance in an Inhomogeneously Broadened Ensemble of Two-Level Systems Coupled to a Low-Q Cavity, Phys. Rev. Lett. **95**, 243602 (2005).

[52] J. Schachenmayer, C. Genes, E. Tignone, and G. Pupillo, Cavity-Enhanced Transport of Excitons, Phys. Rev. Lett. **114**, 196403 (2015).

[53] J. Feist and F. J. Garcia-Vidal, Extraordinary Exciton Conductance Induced by Strong Coupling, Phys. Rev. Lett. **114**, 196402 (2015).

[54] E. Orgiu, J. George, J. A. Hutchison, E. Devaux, J. F. Dayen, B. Doudin, F. Stellacci, C. Genet, J. Schachenmayer, C. Genes, G. Pupillo, P. Samorì, and T. W. Ebbesen, Conductivity in organic semiconductors hybridized with the vacuum field, Nat. Mater. **14**, 1123 (2015).

[55] K. Nagarajan, J. George, A. Thomas, E. Devaux, T. Chervy, S. Azzini, K. Joseph, A. Jouaiti, M. W. Hosseini, A. Kumar, C. Genet, N. Bartolo, C. Ciuti, and T. W. Ebbesen, Conductivity and photoconductivity of a p-type organic semiconductor under ultrastrong coupling, ACS Nano **14**, 10219 (2020).

[56] G. G. Rozenman, K. Akulov, A. Golombek, and T. Schwartz, Long-range transport of organic exciton-polaritons revealed by ultrafast microscopy, ACS Photon. **5**, 105 (2018).

[57] V. Coropceanu, J. Cornil, D. A. da Silva Filho, Y. Olivier, R. Silbey, and J.-L. Brédas, Charge transport in organic semiconductors, Chem. Rev. **107**, 926 (2007).

[58] A. González-Tudela, P. A. Huidobro, L. Martín-Moreno, C. Tejedor, and F. J. García-Vidal, Theory of Strong Coupling between Quantum Emitters and Propagating Surface Plasmons, Phys. Rev. Lett. **110**, 126801 (2013).

[59] T. Botzung, D. Hagenmüller, S. Schütz, J. Dubail, G. Pupillo, and J. Schachenmayer, Dark state semilocalization of quantum emitters in a cavity, Phys. Rev. B **102**, 144202 (2020).

[60] P. W. Anderson, Absence of Diffusion in Certain Random Lattices, Phys. Rev. **109**, 1492 (1958).

[61] F. Evers and A. D. Mirlin, Anderson transitions, Rev. Mod. Phys. **80**, 1355 (2008).

[62] N. C. Chávez, F. Mattiotti, J. A. Méndez-Bermúdez, F. Borgonovi, and G. L. Celardo, Disorder-Enhanced and Disorder-Independent Transport with Long-Range Hopping: Application to Molecular Chains in Optical Cavities, Phys. Rev. Lett. **126**, 153201 (2021).

[63] G. D. Scholes, Polaritons and excitons: Hamiltonian design for enhanced coherence, Proc. R. Soc. A **476**, 20200278 (2020).

[64] G. Engelhardt and J. Cao, Unusual dynamical properties of disordered polaritons in micocavities, arXiv:2112.04060.

[65] C. Gonzalez-Ballestero, J. Feist, E. Gonzalo Badía, E. Moreno, and F. J. Garcia-Vidal, Uncoupled Dark States Can Inherit Polaritonic Properties, Phys. Rev. Lett. **117**, 156402 (2016).

[66] F. Herrera and J. Owrutsky, Molecular polaritons for controlling chemistry with quantum optics, J. Chem. Phys. **152**, 100902 (2020).

[67] M. O. Scully and M. S. Zubairy, *Quantum Optics* (Cambridge University Press, Cambridge, 1997).

[68] E. B. Bogomolny, U. Gerland, and C. Schmit, Models of intermediate spectral statistics, Phys. Rev. E **59**, R1315 (1999).

[69] J. Edwards and D. Thouless, Numerical studies of localization in disordered systems, J. Phys. C **5**, 807 (1972).

[70] F. Wegner, Inverse participation ratio in $2+\varepsilon$ dimensions, Z. Phys. B **36**, 209 (1980).

[71] F. Evers and A. D. Mirlin, Fluctuations of the Inverse Participation Ratio at the Anderson Transition, Phys. Rev. Lett. **84**, 3690 (2000).

[72] T. C. Halsey, M. H. Jensen, L. P. Kadanoff, I. Procaccia, and B. I. Shraiman, Fractal measures and their singularities: The characterization of strange sets, Phys. Rev. A **33**, 1141 (1986).

[73] A. D. Mirlin, Y. V. Fyodorov, F.-M. Dittes, J. Quezada, and T. H. Seligman, Transition from localized to extended eigenstates in the ensemble of power-law random banded matrices, Phys. Rev. E **54**, 3221 (1996).

[74] A. D. Mirlin, Y. V. Fyodorov, A. Mildenberger, and F. Evers, Exact Relations between Multifractal Exponents at the Anderson Transition, Phys. Rev. Lett. **97**, 046803 (2006).

[75] R. Abou-Chacra, D. Thouless, and P. Anderson, A selfconsistent theory of localization, J. Phys. C **6**, 1734 (1973).

[76] S. Leslie, N. Shenvi, K. R. Brown, D. M. Stamper-Kurn, and K. B. Whaley, Transmission spectrum of an optical cavity containing n atoms, Phys. Rev. A **69**, 043805 (2004).

[77] J. L. D'Amato and H. M. Pastawski, Conductance of a disordered linear chain including inelastic scattering events, Phys. Rev. B **41**, 7411 (1990).

[78] D. Bohm and D. Pines, A collective description of electron interactions: III. Coulomb interactions in a degenerate electron gas, Phys. Rev. **92**, 609 (1953).

[79] G. Zhu, S. Schmidt, and J. Koch, Dispersive regime of the Jaynes–Cummings and Rabi lattice, New J. Phys. **15**, 115002 (2013).

[80] H. Haug and A.-P. Jauho, *Quantum Kinetics in Transport and Optics of Semiconductors* (Springer, Berlin, 2008).

[81] D. Hagenmüller, S. Schütz, J. Schachenmayer, C. Genes, and G. Pupillo, Cavity-assisted mesoscopic transport of fermions: Coherent and dissipative dynamics, Phys. Rev. B **97**, 205303 (2018).

[82] M. Pourfath, *The Non-Equilibrium Green's Function Method for Nanoscale Device Simulation* (Springer, Wien, 2014).